

1994

The measurement and modeling of carbon isotope fractionation during thermal degassing of magnesium oxide

Thomas D. Gutierrez
San Jose State University

Follow this and additional works at: https://scholarworks.sjsu.edu/etd_theses

Recommended Citation

Gutierrez, Thomas D., "The measurement and modeling of carbon isotope fractionation during thermal degassing of magnesium oxide" (1994). *Master's Theses*. 838.

DOI: <https://doi.org/10.31979/etd.w8rh-uxuf>

https://scholarworks.sjsu.edu/etd_theses/838

This Thesis is brought to you for free and open access by the Master's Theses and Graduate Research at SJSU ScholarWorks. It has been accepted for inclusion in Master's Theses by an authorized administrator of SJSU ScholarWorks. For more information, please contact scholarworks@sjsu.edu.

INFORMATION TO USERS

This manuscript has been reproduced from the microfilm master. UMI films the text directly from the original or copy submitted. Thus, some thesis and dissertation copies are in typewriter face, while others may be from any type of computer printer.

The quality of this reproduction is dependent upon the quality of the copy submitted. Broken or indistinct print, colored or poor quality illustrations and photographs, print bleedthrough, substandard margins, and improper alignment can adversely affect reproduction.

In the unlikely event that the author did not send UMI a complete manuscript and there are missing pages, these will be noted. Also, if unauthorized copyright material had to be removed, a note will indicate the deletion.

Oversize materials (e.g., maps, drawings, charts) are reproduced by sectioning the original, beginning at the upper left-hand corner and continuing from left to right in equal sections with small overlaps. Each original is also photographed in one exposure and is included in reduced form at the back of the book.

Photographs included in the original manuscript have been reproduced xerographically in this copy. Higher quality 6" x 9" black and white photographic prints are available for any photographs or illustrations appearing in this copy for an additional charge. Contact UMI directly to order.

U·M·I

University Microfilms International
A Bell & Howell Information Company
300 North Zeeb Road, Ann Arbor, MI 48106-1346 USA
313/761-4700, 800/521-0600



Order Number 1359021

**The measurement and modeling of carbon isotope fractionation
during thermal degassing of magnesium oxide**

Gutierrez, Thomas Dominic, M.S.

San Jose State University, 1994

Copyright ©1994 by Gutierrez, Thomas Dominic. All rights reserved.

U·M·I
300 N. Zeeb Rd.
Ann Arbor, MI 48106



THE MEASUREMENT AND MODELING OF
CARBON ISOTOPE FRACTIONATION
DURING THERMAL DEGASSING OF MAGNESIUM OXIDE

A Thesis

Presented to

The Faculty of the Department of Physics

San Jose State University

In Partial Fulfillment

of the Requirements for the Degree

Master of Science

By

Thomas D. Gutierrez

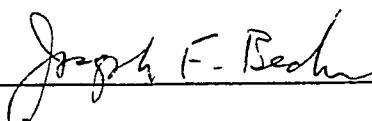
August 1994

© 1994

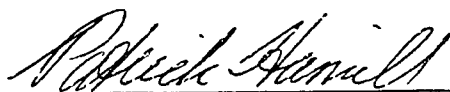
Thomas D. Gutierrez

ALL RIGHTS RESERVED

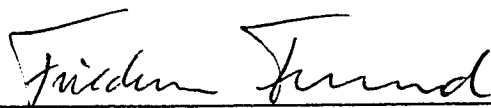
APPROVED FOR THE DEPARTMENT OF PHYSICS



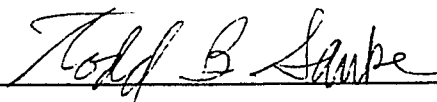
Dr. Joseph F. Becker



Dr. Patrick Hamill

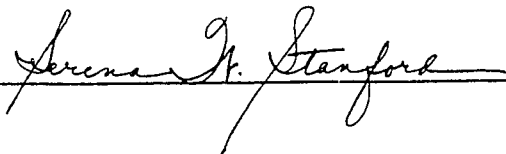


Dr. Friedemann Freund



Dr. Todd B. Sauke

APPROVED FOR THE UNIVERSITY



ABSTRACT

THE MEASUREMENT AND MODELING OF CARBON ISOTOPE FRACTIONATION DURING THERMAL DEGASSING OF MAGNESIUM OXIDE

by Thomas D. Gutierrez

This thesis attempts to confirm the presence of solute carbon in magnesium oxide crystals. A diffusion model was developed which describes the diffusion-limited behavior of carbon in magnesium oxide. Since the diffusion coefficient of ^{13}C is less than that of ^{12}C , this model predicted a time-dependent isotopic fractionation of the carbon leaving the crystal after heating.

Data were acquired using a tunable diode laser spectrometer which measured the isotopic fractionation of the isotopes of carbon in carbon dioxide degassing from magnesium oxide powder after rapid heating. These data were then compared to the results of the diffusion model.

No time-dependent isotopic fractionation was detected to an accuracy of $\pm 0.125\%$. Since the diffusion model predicted isotopic fractionation as great as $\pm 2\%$, it would appear that no solute carbon exists in magnesium oxide. However, because of the sample age, surface chemistry may have occurred, masking the fractionation effect.

Acknowledgments

I would like to dedicate this thesis to my father whose vision of the world serves as a constant inspiration to me in my life. I would like to thank my mother and two brothers, Vince and Leo, for their ongoing support of me and my work. In addition, I would like to thank my thesis advisor Dr. Joseph Becker for his constant support, inspiration, and friendship over the years. Also, I thank the remaining members of my committee, Dr. Todd Sauke, Dr. Friedemann Freund, and Dr. Patrick Hamill, for their ever-present patience, support, and friendship. Finally, I extend a warm thanks to all the family, friends, and teachers who, over the years, have provided for me the context in which to pursue my goals.

Contents

1 INTRODUCTION	1
1.1 Introduction	1
1.2 Theoretical Background	3
2 DIFFUSION	6
2.1 Diffusion Theory	6
2.2 Numerical Methods	13
3 EXPERIMENTAL METHODS	19
3.1 Instrumentation	19
3.2 Experimental Details.	25
3.3 Experimental Parameters and Assumptions	29
4 RESULTS	32
4.1 Modeling Results	32
4.2 Data Results	34
5 DISCUSSION	36
6 CONCLUSION	41
7 FIGURES	43
8 REFERENCES	64

List of Figures

Figure 1 . . . Theoretical segregation profile of carbon in a MgO crystal of radius 100 micrometers.

Figure 2 . . . The enthalpy of segregation for the segregation profile in Figure 1.

Figure 3 . . . A Newtonian heating profile with a characteristic heating time of 1000 seconds.

Figure 4 . . . A schematic of the Stable Isotope Laser Spectrometer.

Figure 5 . . . A typical evacuated scan with a blanking pulse.

Figure 6 . . . A typical etalon scan with a blanking pulse.

Figure 7 . . . A schematic of some CO₂ absorbance bands in the 2310 cm⁻¹ region.

Figure 8 . . . Transmission as a function of wavenumber for a scan across the spectral lines of interest.

Figure 9 . . Plots for the cases of instant and non-instant heating for a modeled $^{13}\text{C}/^{12}\text{C}$ ratio as a function of time resulting from diffusion in the potential from Figure 2.

Figure 10 . . Ten plots of the modeled carbon profile inside MgO plotted for 1000 second intervals for a total of 10000 seconds resulting from diffusion in the potential from Figure 2.

Figure 11 . . Plots for the cases of instant and non-instant heating for modeled carbon leaving the crystal per unit time as a function of time resulting from diffusion in the potential from Figure 2.

Figure 12 . . Plots for the cases of instant and non-instant heating for a modeled $^{13}\text{C}/^{12}\text{C}$ ratio as a function of time resulting from diffusion in a constant potential.

Figure 13 . . Ten plots of the modeled carbon profile inside MgO plotted for 1000 second intervals for a total of 10000 seconds resulting from diffusion in a constant potential.

Figure 14 . . Plots for the cases of instant and non-instant heating for modeled carbon leaving the crystal per unit time as a function of time resulting from diffusion in a constant potential.

Figure 15 . . Carbon dioxide leaving the crystal per unit time as a function of time for sequence one data (15 grams of MgO heated to 377°C).

Figure 16 . . $^{13}\text{C}/^{12}\text{C}$ ratio as a function of time for sequence one data (15 grams of MgO heated to 377°C).

Figure 17 . . Carbon dioxide leaving the crystal per unit time as a function of time for sequence two data (7.5 grams of MgO heated to 400°C).

Figure 18 . . $^{13}\text{C}/^{12}\text{C}$ ratio as a function of time for sequence two data (7.5 grams of MgO heated to 400°C).

Figure 19 . . $^{13}\text{C}/^{12}\text{C}$ ratio as a function of time for sequence three data.

Figure 20 . . A scatter plot of all data sequences together.

Chapter 1

Introduction

1.1 Introduction

This thesis is a continuation of the investigation of the presence and behavior of carbon in magnesium oxide crystals. The investigation consisted of theoretical and experimental improvements over ideas originally developed by F. Freund.^{1,2} The motivation of this thesis is to present the next generation of experimental and theoretical developments over previous methodologies. The basis of the experiments and ideas pursued by this and other related works requires some background as follows.

A process of geological and geophysical interest is the evolution of carbon dioxide gas during the heating of minerals and rocks. For example, when a carbonate such as MgCO_3 is heated, it releases CO_2 . However, non-carbonate minerals, after having crystallized from a melt containing CO_2 , may take up CO_2 in solid solution (*i.e.*, dissolve CO_2 in the crystal structure). Because of its simple crystal structure, magnesium oxide grown from a CO_2 saturated melt in a carbon-arc furnace provides an excellent non-carbonate model system in which to study CO_2 in solid solution.

The release of CO_2 during rapid heating of arc-fusion grown MgO , ground to a coarse powder, has been observed. However, the source of the CO_2 is the

subject of some controversy. The MgO grains may be carbonated at the surface due to reaction with atmospheric CO₂ so that upon heating, CO₂ is released. This would be called "contamination." However, even when surface contamination has been avoided or minimized, significant amounts of CO₂ are still detected upon heating. This suggests that there may be some process not involving surface contamination by which CO₂ can degas from MgO. If such a process for degassing exists, the question arises: can it be distinguished from surface contamination?

A mechanism has been suggested^{1,2} by which structurally dissolved carbon could diffuse from the interior of the crystal to the surface and form carbon dioxide, carbon monoxide, and possibly hydrocarbons. If this process is diffusion-limited, diffusion theory predicts the time dependence of the evolution of the stable isotopes of carbon (¹³C and ¹²C) of the gases from the surface. By contrast, if the surface of MgO is carbonated (either by reaction with gaseous CO₂ in the atmosphere or as a result of completed segregation from the bulk), the evolving CO₂ is expected to show no time dependent ¹³C/¹²C fractionation. Thus, by measuring the ¹³C/¹²C ratio of the CO₂ gas evolved from MgO as a function of time during and following rapid heating, and comparing it to a diffusion model, information about the nature of the carbon in the crystal lattice may be obtained.

To measure the ¹³C/¹²C ratio in CO₂ evolved from MgO samples, the Stable Isotope Laser Spectrometer (SILS) at NASA Ames Research Center was used.³ The SILS has been developed and was previously used to measure carbon isotope ratios in CO₂ gas to an accuracy of ±0.2% and a precision of ±0.1%. The SILS instrument currently offers features such as measurement speed, accuracy, and minimal required sample purification for the measurement of carbon isotopic compositions in samples of CO₂. This facilitates both extraterrestrial

and terrestrial *in situ* measurements which are of interest in the space, atmospheric, earth, and life sciences. The SILS instrument provides an ideal means by which to measure accurately the stable carbon isotopic ratios of CO₂ evolved from heated MgO as a function of time.

1.2 Theoretical Background

The work presented in this thesis has been motivated by observations of anomalous behavior in the thermal and electrical properties of simple crystals.^{4,5} For example, the normally insulating MgO has been observed to exhibit enhanced electronic conductivity and to acquire a positive surface charge at elevated temperatures (500°C). According to data obtained by different techniques,^{4,5} this is due to positive hole-type charge carriers, O⁻ states in the O²⁻ matrix, which are generated at 500°C.

F. Freund^{4,5} is exploring the charge carriers in MgO, CaO, and other oxide and silicate crystals using a Charge Distribution Analysis (CDA) experiment. CDA is a technique developed to measure surface charges on crystals as a function of temperature and external electric field gradients. This is achieved by placing a crystal sample on a sensitive balance mounted inside a furnace. The balance is located between a probe and a grounding plate between which a bias voltage can be applied. This generates an electric field gradient through the sample. If surface charges appear on the sample as the temperature is increased, a deflection is recorded by the balance.

How may the presence of carbon in MgO be related to the mobility of O⁻ charge carriers in its lattice? If CO₂ is present during the crystallization of MgO in a CO₂-rich gas environment (such as in a carbon arc furnace), CO₂ will

dissolve in the crystal lattice forming a solid solution. As the temperature decreases the solubility range for CO_2 in MgO narrows. As a result, under thermodynamic equilibrium conditions, solute carbon must diffusively segregate to the surface. Eventually, during further cooling, kinetic constraints will restrict the diffusion and prevent the solid solution from achieving thermodynamic equilibrium. At this point, the system becomes a supersaturated solid solution.

To explain the O^- charge carrier mobility in MgO as measured by CDA, a chain of internal dissociation and charge transfer reactions must have taken place involving the CO_2 dissolved in the lattice.¹ Ultimately, C atoms from dissolved CO_2 are believed to reside in interstitial sites bonded to an O^- creating a CO^- anion complex. The other O^- created in the course of these reactions becomes mobile when the MgO is heated.¹ The mobility of O^- charge is not to be regarded as the physical translation of an O^- anion through the MgO lattice, but rather a succession of transfers of defect electrons contained in the O^{2-} anion sublattice in the MgO matrix. The diffusion of cations in the lattice is believed to occur as successive jumps in parallel to the O^- .

Given the above coupled O^- -cation mechanism, the investigation of C in MgO may be important for understanding many different anomalies observed in MgO and other simple crystals during heating. By designing experiments that would critically evaluate the existence of carbon in the MgO lattice, insights into fundamental issues of geophysics and geology may be gained. The observed properties of insulating materials at moderate temperatures may be extended to more complicated crystals. Practical applications of such processes to earthquake precursors are being studied. For example, if temperature and pressure conditions exist such that O^- -type charge carriers are generated prior to an earthquake, an electric current may be detectable in the ground. Other

questions related to the origin of gases emanating from the earth's interior are also being studied. CO_2 and H_2O dissolved in rocks deep in the earth could become supersaturated during cooling and then degas under thermodynamic non-equilibrium conditions leading to, among other things, the formation of organic material.

Chapter 2

Diffusion

2.1 Diffusion Theory

Investigation of the diffusion of carbon in MgO has been previously explored by J. P. Trice.⁶ However, because of the accuracy limitations of both the diffusion model and the experimental isotopic determinations at that time, further investigations were deemed desirable to provide a more complete picture of the physical processes taking place.

The diffusion model of Trice has been altered to include an additional force term. This allows effective modeling of the tendency of solute C to segregate towards crystal grain boundaries. The segregation profile is assumed to be the steady state distribution of C inside a crystal at a given temperature and constant pressure. If no additional forces are operating on the solute carbon inside the crystal, the system would strive for a uniform carbon distribution. However, the form of the segregation profile of carbon in MgO at equilibrium was observed not to be constant,^{1,2} indicating that forces are operating within the crystal which distribute the solute C non-uniformly throughout the crystal. The form of the potential giving rise to this force can be approximated from the measured segregation profile.

When the equilibrium is disturbed (*i.e.*, the crystal is heated) the forces that led to the segregation profile continue to operate. Thus the diffusion of particles in the lattice is modified. This can be modeled as a random walk with unequal probabilities to move in different directions as determined by the local forces in the crystal.

Since a non-uniform carbon segregation profile in MgO has been measured, the addition of a potential term in the diffusion equation was necessary to improve the diffusion model. Thermodynamically, this potential is known as the enthalpy of segregation ΔH_{seg} ⁷ which is composed of a sum of several terms that give rise to a driving force. Such a potential energy is often found in the context of semiconductor theory. An example of the terms which may be involved in describing the enthalpy of segregation are

$$\Delta H_{seg} = \Delta H_{\gamma} + \Delta H_w + \Delta H_e$$

where ΔH_{γ} is the surface energy term, ΔH_w is the binary solution interaction term, and ΔH_e is the elastic solute strain energy. Note, however, it is not necessary to know a precise form of ΔH_{seg} if an experimentally measured segregation profile is known. Figure 1 shows a theoretical segregation profile of C in MgO similar to that which has been measured.¹ This profile has a width of approximately 20 nanometers and a bulk to surface ratio of 0.001. Figure 2 shows a plot of the enthalpy of segregation at a temperature of 300K for the segregation profile in Figure 1.

As discussed above, for some temperature and partial pressure of C at the surface of the crystal (at room temperature in the air, for example) this driving force will cause the system to reach an equilibrium segregation concentration

profile. If the temperature or the pressure are changed, the atoms in the system will diffuse to their new equilibrium state in the presence of this potential.

By first showing how the familiar diffusion equation can be obtained from classical field theory, it will be demonstrated that the diffusion equation of interest can be derived with an appropriate straightforward modification. To the force generated by the chemical potential of the carbon concentration, an additional force generated by the gradient of an arbitrary potential is added. This arbitrary potential can be regarded as the enthalpy of segregation.

Starting with the continuity equation^{8,9}

$$\frac{\partial \rho(\vec{r}, t)}{\partial t} = -\vec{\nabla} \cdot \vec{J}(\vec{r}, t)$$

the density of diffusing material (carbon atoms per unit volume) is set equal to the space and time dependent concentration

$$\rho(\vec{r}, t) = C(\vec{r}, t)$$

The flux is given by

$$\vec{J}(\vec{r}, t) = -\frac{D(\vec{r})C(\vec{r}, t)}{kT} (\vec{\nabla} \mu(\vec{r}, t))$$

where \vec{r} is the position vector, $D(\vec{r})$ is the position dependent diffusion coefficient, k is the Boltzmann constant, and T is the temperature, and $\mu(\vec{r}, t)$ is the chemical potential given by

$$\mu(\vec{r}, t) = kT \ln[C(\vec{r}, t)]$$

By substituting $\mu(\bar{r},t)$ into $\bar{J}(\bar{r},t)$, then $\bar{J}(\bar{r},t)$ into the continuity equation, a "chemical force" flux-conservative diffusion equation with diffusion coefficient $D(\bar{r})$, can be expressed as the negative divergence of the negative gradient of the concentration

$$\frac{\partial C(\bar{r},t)}{\partial t} = -\bar{\nabla} \cdot [D(\bar{r})(-\bar{\nabla} C(\bar{r},t))]$$

Assuming that $D(\bar{r})$ is constant, this becomes the familiar three dimensional diffusion equation

$$\frac{\partial C(\bar{r},t)}{\partial t} = D\nabla^2 C(\bar{r},t)$$

If the crystal is modeled as a sphere and only radial diffusion is considered, the equation becomes one-dimensional in spherical coordinates

$$\frac{\partial C}{\partial t} = \frac{D}{r} \frac{\partial^2 C}{\partial r^2}$$

With the change of variable $U'(r,t) = r C(r,t)$, this becomes a one-dimensional diffusion equation with constant coefficient D ,

$$\frac{\partial U'}{\partial t} = D \frac{\partial^2 U'}{\partial r^2}$$

Using the appropriate initial and boundary conditions, this equation is the diffusion model used by Trice.⁶

To get an expression for the diffusion equation of interest as discussed above, a force term proportional to the gradient of a time independent potential $\bar{\nabla}\phi(\bar{r})$ is added to the flux term from the original continuity equation

$$\bar{J}(\bar{r},t) = -\frac{D(\bar{r})C(\bar{r},t)}{kT} (\bar{\nabla}\mu(\bar{r},t) + \bar{\nabla}\phi(\bar{r}))$$

After substituting $\mu(\bar{r},t)$ into $\bar{J}(\bar{r},t)$ and then $\bar{J}(\bar{r},t)$ back into the continuity equation, the diffusion equation with constant D then becomes

$$\frac{\partial C(\bar{r},t)}{\partial t} = D \left\{ \bar{\nabla} \cdot \left[\bar{\nabla} C(\bar{r},t) + \frac{C(\bar{r},t)}{kT} \bar{\nabla} \phi(\bar{r}) \right] \right\}$$

To derive the form of the enthalpy of segregation given an initial (before heating) segregation profile at equilibrium $C(r,0)$, the steady state solution to the above equation is solved. From this solution the equilibrium segregation profile as a function of a potential is

$$C(r,0) = e^{\frac{-\phi(r)}{kT_{eq}}}$$

where the constant T_{eq} is the initial equilibrium temperature (before heating) and $\phi(r)$ is the enthalpy of segregation, ΔH_{seg} .

This modified diffusion equation in spherical coordinates is

$$\frac{\partial C}{\partial t} = D \left\{ \frac{\partial^2 C}{\partial r^2} + \frac{2}{r} \frac{\partial C}{\partial r} + \frac{1}{kT} \frac{d\phi}{dr} \frac{\partial C}{\partial r} + \frac{2}{kT} \frac{1}{r} \frac{d\phi}{dr} C + \frac{1}{kT} \frac{d^2\phi}{dr^2} C \right\}$$

and using the change of variable $U = Cre^{\frac{\phi}{kT}}$, the equation is transformed into

$$\frac{\partial U}{\partial t} = D \left\{ \frac{\partial^2 U}{\partial r^2} - \frac{1}{kT} \frac{d\phi}{dr} \frac{\partial U}{\partial r} + \frac{1}{kT} \frac{d\phi}{dr} \frac{U}{r} \right\}$$

We have assumed D to be independent of r but in general there will be a dependence on the temperature. For example, using the Arrhenius formula,¹⁰ the diffusion coefficient is

$$D = D_0 e^{\frac{-Q}{kT}}$$

where Q is the local activation energy in the crystal lattice and D₀ is the pre-exponential diffusion coefficient. In addition, from statistical mechanics, the diffusion coefficients of ¹²C and ¹³C will vary by a factor of the square root of their masses so

$$D_{13} = \sqrt{\frac{12}{13}} D_{12}$$

Since the diffusion coefficient is different for each carbon isotope, at a given temperature they will move at different speeds through the lattice. Now, using the same (within a multiplicative factor) initial segregation profile for each carbon isotope and setting the appropriate boundary conditions, the isotopic ratio of the carbon leaving the crystal as a function of time after an instantaneous temperature change can be modeled. If the motion of the carbon atoms is diffusion-limited, isotope fractionation as predicted by this model should be observed during degassing of the crystal.

However, the fact that the heating of the sample is not instantaneous must now be taken into account. The temperature change is instead some

function of time. A simple profile that can be used is one derived assuming Newtonian heating so that the rate of temperature change of the sample from the initial temperature T_i to the environmental temperature T_f is proportional to the difference between the environmental temperature and the temperature T at time t

$$\frac{dT(t)}{dt} = -\gamma(T(t) - T_f)$$

The solution of which is

$$T(t) = T_f + Ae^{-\gamma t}$$

With the initial condition

$$T(0) = T_i$$

the constant of integration A is

$$A = (T_i - T_f)$$

So finally, the Newtonian temperature profile $T(t)$ is

$$T(t) = T_f + (T_i - T_f) e^{-\gamma t}$$

Figure 3 shows a typical Newtonian temperature profile for a sample from changing temperature from 300K to 700K with a characteristic heating time of 1000 seconds. In general, the temperature profile is not expected to be purely Newtonian. When the crystal degasses this is expected to have the effect of

cooling the sample. As more CO₂ is released, the temperature of the sample may tend to deviate from a Newtonian profile as the cooling due to degassing and the heating of the sample will conflict. An experiment could be conducted to discover empirically the temperature of the crystal as a function of time. However, for simplicity, the profile was assumed to be Newtonian. Assuming carbon is diffusing inside the crystal, the degree of non-Newtonian behavior can be seen by comparing the differences in carbon leaving the crystal as a function of time as predicted by the model and the amount of carbon leaving the crystal as measured experimentally

The Newtonian temperature profile can now be inserted into the diffusion equation. So finally

$$\frac{\partial U}{\partial t} = D_0 e^{-\frac{Q}{kT(t)}} \left\{ \frac{\partial^2 U}{\partial r^2} - \frac{1}{kT(t)} \frac{d\phi}{dr} \frac{\partial U}{\partial r} + \frac{1}{kT(t)} \frac{d\phi}{dr} \frac{U}{r} \right\}$$

2.2 Numerical Methods

Because of the form of the time-dependent temperature, the diffusion equation above is not separable into the product of a radial solution and a temporal solution. In addition, because of the form of the initial concentration profile (see section 3.3), there exists a non-removable singularity at $r=0$, which disallows a Taylor expansion about the origin for purposes of analytical approximations. Thus, an analytical solution for this diffusion model was not pursued. Instead, a three-point, forward-time centered-space (FTCS) explicit numerical approximation scheme written in Interactive Data Language

(Research Systems Inc., Boulder, CO) was used to approximate the partial differential equation.^{11,12}

Using this scheme

$$\frac{\partial U(r, t)}{\partial t} = D_0 e^{\frac{-Q}{kT(t)}} \left\{ \frac{\partial^2 U(r, t)}{\partial r^2} - \frac{1}{kT(t)} \frac{d\phi(r)}{dr} \frac{\partial U(r, t)}{\partial r} + \frac{1}{kT(t)} \frac{d\phi(r)}{dr} \frac{U(r, t)}{r} \right\}$$

can be approximated by the finite difference equation

$$U_j^{n+1} = F_1(r, \Delta r, \Delta t, t) U_{j+1}^n + F_2(r, \Delta r, \Delta t, t) U_j^n + F_3(r, \Delta r, \Delta t, t) U_{j-1}^n$$

where

$$U(r, t) = C(r, t) r e^{\frac{\phi(r)}{kT(t)}}$$

and $C(r, t)$ represents the carbon concentration as a function of time and the radial distance from the center of the crystal modeled as a sphere. The notation U_j^n is the discrete value of $U(r, t)$ at the radial grid-point j and at time-step n .

The functions F_1 , F_2 , and F_3 are defined as follows:

$$F_1(r, \Delta r, \Delta t, t) = \frac{D_0 e^{\frac{-Q}{kT(t)}} \Delta t}{\Delta r^2} \left(1 - \frac{\Delta r}{2kT(t)} \phi'(r) \right)$$

$$F_2(r, \Delta r, \Delta t, t) = 1 - 2 \frac{D_0 e^{\frac{-Q}{kT(t)}} \Delta t}{\Delta r^2} \left(1 - \frac{\Delta r^2}{2rkT(t)} \phi'(r) \right)$$

$$F_3(r, \Delta r, \Delta t, t) = \frac{D_0 e^{\frac{-Q}{kT(t)}} \Delta t}{\Delta r^2} \left(1 + \frac{\Delta r}{2kT(t)} \phi'(r) \right)$$

where

$$\phi'(r) = \frac{d\phi(r)}{dr}$$

and Δr and Δt are the grid spacing for the radial and time-axes, respectively. Since the FTCS method is only conditionally stable, a von Neumann stability analysis was used to determine a stability criterion.^{11,12} The von Neumann stability analysis seeks a relationship between parameters of the system such that numerically oscillatory solutions of all frequencies between spatial grid points decay in time. To achieve this, an eigenmode solution is assumed of the form

$$U_j^n = \xi^n e^{-i(kj\Delta r)}$$

where n and j still serve their roles as the time and space grid point indices. However, the ξ^n term represents a complex number ξ to the n^{th} power, whereas U_j^n represents U evaluated at the n^{th} and j^{th} grid points. By inserting the above equation into the finite difference equation above and solving for Δt in terms of the other parameters of the equation (*i.e.* T , Q , D_o , $\phi'(r)$, and Δr) such that $|\xi| \leq 1$ for all wavenumbers k , the stability criterion can be obtained.

Using Mathematica (Wolfram Research, Champaign, IL) to evaluate the eigenmode solution, the stability relationship between Δr and Δt was found to be

$$\Delta t \leq \frac{2e^{\frac{Q}{kT(t)}}}{D_o \left[\frac{4}{\Delta r^2} - \frac{\phi'(r)}{kT(t)r} \right]}$$

To facilitate a more accurate modeling of sharp features near crystal boundary regions (where early-time sharp features reside), the radial axis was divided into N regions with each successive region toward the crystal boundary having the same number of points but half the length and thus twice the point density. The last region, however, has the same length as the next to last region. This process renders the spatial grid spacing Δr not constant across the crystal.

Since Δr , $T(t)$, and $\phi'(r)$ are not constant and the stability criterion is a function of these parameters, worst case values were chosen for insertion into the stability criterion. This determined the largest allowed Δt which achieved stability for all parameters.

The stability criterion was verified by confirming the stability of solutions for various values of Δt about the stability criterion. When the stability criterion was violated (*i.e.*, Δt was too large), solutions clearly oscillated and were amplified. When the exact value of Δt as recommended by the stability criterion was used, the solution still oscillated but damped away slowly. As smaller values of Δt were used, the oscillations died away more rapidly. When the value of Δt was half of the value recommended by the stability criterion, no visible oscillations were detected. Thus, to eliminate oscillations in the solutions, Δt was chosen to be between a factor of two and a factor of ten smaller than that required by the stability criterion.

The precision of the solution was confirmed by systematically choosing highly resolved radial regions and the time-axis resolutions were chosen well within that required by stability. The various stable solutions for different time and space resolutions were then observed to diverge only for early times generally outside the realm of experimental capabilities. If differences in the solutions between various degrees of resolution did exist for times comparable to

experimental times, the general features tended to be very similar while the exact numbers varied. However, reasonable care was taken to maximize the resolution of the space and time axis such that over the period of a modeled experiment minimal error was introduced.

The goal in this technique was not to visualize the behavior of carbon inside the crystal but rather to ensure the accuracy of the outgassing of carbon so that modeled experiments and actual measurements could be compared. However, the diffusive behavior of the carbon *inside* the crystal under the influence of different forces does prove to be interesting, as pointed out by Trice.⁶ Indeed, this model for carbon inside a crystal could be extended to the modeling of other more general systems in which diffusion limited behavior is occurring under the influence of internal or external forces.

To determine the isotopic ratio of the carbon leaving the crystal, the value of $U(r,t)$ inside the crystal at a particular time-step was first transformed back into the carbon concentration $C(r,t)$. The total amount of carbon of a particular isotope i , leaving the crystal in the time $\Delta t = t_2 - t_1$ (where $t_2 > t_1$) is then

$$CarbonOut_i(\Delta t) = \iiint_{InTheCrystal} [C_i(r, t_1) - C_i(r, t_2)] r^2 \sin \theta dr d\theta d\phi$$

The theoretical, time dependent, isotopic ratio of carbon degassing isothermally from within MgO is

$$\frac{CarbonOut_{13}(\Delta t)}{CarbonOut_{12}(\Delta t)}$$

evaluated for all time steps.

The parameters of this model are the pre-exponential diffusion coefficient D_0 , the activation energy Q , the characteristic heating time γ^{-1} , the radius of the crystal grains and the characteristics of the initial segregation profile. Since only preliminary information about these parameters was available, a set of these parameters was sought such that the model could best fit the experimental data. An approximate experimental verification of the time dependent carbon isotope fractionation following the predictions of this model, given some choice of reasonable parameters, may demonstrate the presence of carbon within the crystal structure of MgO. This would eliminate surface contamination as the unique source of carbon during degassing.

Chapter 3

Experimental Methods

3.1 Instrumentation

The SILS instrument used to measure the $^{13}\text{C}/^{12}\text{C}$ ratio is a lead-salt tunable diode laser spectrometer operating near the 4.3 micrometer region.^{3,13,14} Lead-salt tunable diode lasers (TDL) emit with a very narrow line width of approximately 0.0001 cm^{-1} . Using a TDL spectrometer it is thus possible to resolve and to measure the absorbance of individual rotational spectral lines within the vibrational bands of carbon dioxide. This information can then be used to determine carbon isotopic content of an unknown sample relative to a known sample.

To measure the relative abundance of the carbon isotopes, a ratiometric method is used. Proximate absorption lines representing $^{12}\text{CO}_2$ and $^{13}\text{CO}_2$ (regardless of their angular momentum -- though lines with smaller J quantum numbers and non-"hot band" lines are generally less sensitive to temperature) are chosen such that their absorbances are nearly equal. The isotopic enhancement of a sample is then determined relative to a known reference gas, whose spectra are taken simultaneously. This method of measurement is known as a ratiometric technique.

The reasons for using ratiometric techniques are important. Perhaps an alternate method would be to *directly* measure the isotopic ratio of $^{13}\text{C}/^{12}\text{C}$ in a sample (*i.e.*, determining the isotopic ratio of $^{13}\text{C}/^{12}\text{C}$ using only the spectra from the sample in question). For example, to eliminate the temperature dependence of the strengths due to differing J quantum numbers, the integrated absorbances of corresponding rotational lines (*i.e.*, individual absorption lines having the same total angular momentum quantum numbers and branch specifications in their respective vibrational band of $^{12}\text{CO}_2$ or $^{13}\text{CO}_2$) might be compared. In this method, the task of tuning the laser to scan over 50 cm^{-1} to compare two lines whose absorbances may vary by two orders of magnitude would be formidable. In addition, the large numbers of intermediate absorption lines as well as problems due to the greatly differing signal strengths for the two isotopes could make data analysis complicated.

If these problems could be overcome and if all absorbance characteristics of $^{12}\text{CO}_2$ and $^{13}\text{CO}_2$ were identical, the direct comparison of such lines would yield the ratio of $^{13}\text{C}/^{12}\text{C}$ in the sample. However, in general, all absorbance characteristics which contribute to the measured strengths are not identical in $^{12}\text{CO}_2$ and $^{13}\text{CO}_2$. For example, the optical collision cross section and state population factors will be different owing to the isotopic mass differences. This will cause the ratio of integrated absorbances to be unequal to the relative abundance of $^{13}\text{C}/^{12}\text{C}$.

The ratiometric method must be used to avoid these problems. By taking the ratio of absorbances in a sample gas and dividing them by the ratio of the absorbances of the same lines in a known reference gas, the final number is equal to the relative isotopic enhancement of $^{13}\text{C}/^{12}\text{C}$. In this method all differences are divided out in the ratioing. In addition, unlike the direct method,

the lines which are used need not be of equal J quantum number and thus may be proximate for convenience of measurement.

The SILS uses multiple beams for simultaneous acquisition of spectra from a sample cell, reference cell, evacuated cell, and an etalon.³ The simultaneous acquisition of the calibration beams (etalon and evacuated) with each data scan, in conjunction with an initial all-evacuated scan, compensate for drifts in the instrument over the period of an experiment. A scan is a term used to describe a set of signal averaged sweeps where a sweep is one cycle of the laser over the spectral range of interest. Figure 4 shows a schematic of the SILS instrument.³ The laser is a liquid nitrogen cooled lead-salt tunable diode laser (Model L5621 Laser Photonics, Andover, MA 01810). The detectors (labeled "Det." in Figure 4) are liquid nitrogen cooled indium antimonide detectors. The etalon is a solid germanium Fabry-Perot etalon. The pellicle beam splitters and mirrors direct the laser light to the evacuated, etalon, reference, and sample detectors respectively. The detectors then send their respective signals to individual preamplifiers. The final signals are then collected and processed by an 80486 based IBM PC compatible computer.

Calibration scans are important for proper analysis. The evacuated beam gives the data analysis software information about the system when 100% of the laser light is transmitted. A "blanking pulse" is inserted at the beginning of each sweep using a function generator which turns off the laser for approximately 5 ms during a scan. This provides 0% transmission spectral data. Combining the information from the evacuated channel and the blanking pulse permits proper normalization of the data. Figure 5 shows a typical evacuated scan with a blanking pulse. The etalon beam contains a germanium etalon with a free spectral range of 0.04822 cm^{-1} . This gives the analysis software information which allows it to determine and linearize the frequency axis of a scan. The free

spectral range of an etalon is essentially the spacing in wavenumbers between interference fringes. Figure 6 shows a typical etalon scan.

In general, each set of scans contains its own set of calibration scans. This can compensate for inaccuracies in data due to long term drifts of the instrument such as thermal drifts in the room and variations in purging gas as a function of time. Nitrogen gas, which has no absorption features near the spectroscopic region of interest, is used to purge the spectrometer of atmospheric CO₂. However, if the experiment requires only a few sets of scans and is thus performed over a reasonably short time period (< 30 minutes), then an initial set of calibration scans is all that is required. For such an experiment, using individual calibration scans *versus* using an initial calibration scan have a negligible effect on the values of the isotopic ratios within the measurement error bars.

Instrument response function (IRF) distortions lead to inaccuracies in the extraction of line parameters which ultimately create errors in the isotopic ratio measurements. Knowledge of the IRF for the SILS has been incorporated into the data analysis program as described below.

The IRF of the SILS has been previously studied by V. V. Dinh.¹⁵ The primary constituents of the SILS IRF are approximated by a Gaussian and a Lorentzian component. The effect of the IRF is to further broaden the already temperature and pressure broadened spectral lines which limits the accuracy and precision of the carbon isotope ratio measurements. The Lorentzian component is simply the frequency line width of the laser. A technique developed by Podolske and Sauke¹⁶ measures the Lorentzian width of the IRF. Using this technique, the Lorentz width was measured to vary linearly with inverse power as predicted by Schalow and Townes.¹⁷ The Lorentz width, and

thus the best possible resolution of a spectral line at a typical laser power, is approximately 0.0001 cm^{-1} .

The Gaussian component of the IRF is due to AM noise on the driver current manifesting itself as FM noise on the laser output (being tunable, the output frequency of the laser is a function of the input current). The noise is known to be only approximately Gaussian because of 60 Hz line interference in the circuitry of the current driver. However, a data acquisition feature called a "tracker" (described below) removes most of the 60 Hz interference leaving mostly a Gaussian noise distribution. Present estimates of the Gaussian width of the IRF are 0.0003 cm^{-1} . Although this is about ten times smaller than the typical Doppler width of a measured spectral line, it can be shown that this creates a significant distortion in line shape.

In order to narrow the Gaussian width of the IRF, a data acquisition tracking feature was used. The tracker, in brief, "locks on" to a user specified line and proceeds to shift entire subsequent sweeps to the original "lock on" position. This is done so that slow frequency drifts such as small temperature drifts of the laser, which may arise over the period of the user specified number of scans, are eliminated prior to signal averaging. Using the tracker, the Gaussian width of the IRF is effectively reduced to 0.0001 cm^{-1} .

Once data have been collected, an analysis program extracts various line parameters, including the integrated absorbances, and makes them available in a file. The analysis program utilizes a Marquart-Levenberg chi-square minimization algorithm.¹¹ The procedure iteratively minimizes the chi-square of a fit by adjusting various specified parameters. An initial estimate of each parameter is also required.

Since the spectra are measured in transmittance and the parameters of interest are in absorbance space, an analytical relationship between the

measured data and the line parameters can be obtained from Beer's Law. The basic analytical expression which describes the data in transmittance is³

$$T(\nu) = B(\nu) + e^{-\sum_i [S_i \times V(D_i, L_i, \nu - \nu_i)]}$$

where the sum is over all lines present in the scanned set of spectral data. S_i is the integrated absorbance, ν_i is the frequency position, and V is the Voigt function. The Voigt function is defined as the convolution of a Gaussian of width D_i and a Lorentzian of width L_i . The Gaussian and Lorentzian shapes are due to Doppler and collision broadening mechanisms respectively. $B(\nu)$ is a linear baseline term which includes slope and intercept parameters. $B(\nu)$ models instrumental effects which are not explicitly derivable from Beer's Law.

In general, more parameters can be added to the above equation and further incorporated into the fitting model, as long as the partial derivatives of the new parameters can be obtained. For example, a parabolic term may be included in $B(\nu)$ to account for broad curvature of the baseline. Sinusoidal fringes due to optical interference in a particular optical path in the spectrometer may also be included in the model.

However, as discussed above, the IRF distorts the data from the form as described by $T(\nu)$ above. The analytical function $M(\nu)$ which is fitted to the data as *measured*, is obtained by convolving $T(\nu)$ given above with the IRF:

$$M(\nu) = V_{IRF}(G_{IRF}, L_{IRF}, \nu - \nu') * T(\nu')$$

where V_{IRF} is a Voigt function generated by the convolution of the Gaussian and Lorentzian components of the IRF and the asterisk (*) indicates a convolution of the IRF with the undistorted spectra $T(\nu')$.

Finally, the fitting program finds a best fit to $M(\nu)$ given the values of G_{IRF} and L_{IRF} by the user. The fitting parameters the program uses to achieve the best fit on a single line are: the absorbance S_i , the Lorentz width L_i , the Doppler width D_i , and the line position ν_i . Global fitting variables used for all lines in a set of spectra include the slope and intercept of the baseline in $B(\nu)$.

Since M is also a function of the IRF parameters, it might be tempting to use the fitting program to find the best fit to the data using the IRF parameters as additional fitting parameters. However, this is not necessary since the parameters of the IRF can be measured accurately and independently of the data.

3.2 Experimental Details

To collect CO_2 gas samples, a given amount of MgO powder in an evacuated glass bulb were quickly heated from room temperature to the desired temperature in a thermally controlled molten metal bath. The MgO was from a jar stored in ambient air for more than 3 years. The grains were of nearly equal size (75-125 micrometers in diameter). The evolved gases were passed through a methanol/dry-ice trap at -80°C to remove water. Other gases, including CO_2 , not trapped in the methanol/dry-ice trap, were then trapped in a liquid nitrogen trap. Any remaining non-condensable gases (H_2 , CO , and CH_4) were subsequently pumped away. The gas collected in the nitrogen trap, most of which is carbon dioxide, was then warmed-up and cryopumped with liquid nitrogen into glass tubes, sealed, and labeled by date and time. Each sample was collected over a time interval increasing approximately with time squared. Three sets of gas samples (sequence one, sequence two, and sequence three) were generated from three different amounts of MgO . The final sets of collected gas

each represented several hours of CO₂ evolution from the crystals. The corresponding isotopic fractionation of each sample was determined on the SILS instrument as described above.

To measure the isotopic ratio on the SILS instrument, the glass tubes were cleaned with methanol, broken in a vacuum, and cryopumped into a gas handling manifold. Approximately 2.00 Torr of gas from an individual sample in the manifold was then released into the sample cell of the SILS instrument. If the trap for a particular sample contained more than 2.00 Torr, the excess gas was subsequently cryopumped back into the trap from the sample cell. If the trap originally contained less than 2.00 Torr, then the gas was analyzed using that amount. The samples typically had no less than 1.50 Torr. As a reference gas, standard industrial CO₂ was used. The pressure in the reference cell was matched to the pressure of the sample cell within 0.01 Torr.

The temperature and current of the laser were selected so that the laser scanned over a region containing known rovibrational lines of ¹²C¹⁶O¹⁶O*, ¹²C¹⁶O¹⁷O, ¹²C¹⁶O¹⁸O, ¹²C¹⁶O¹⁶O* and ¹³C¹⁶O¹⁶O, where the asterisk (*) indicates that the ¹²C¹⁶O¹⁶O* is a "hot band" line *not* making a transition from a ground vibrational state to the first excited state.

This spectral region near 2310 cm⁻¹ has been commonly used by the SILS project for measuring both ¹³C/¹²C and ¹⁸O/¹⁶O isotopic ratios.³ Figure 7 shows a schematic of the spectral region of interest. This region contains several overlapping bands of the ν_3 vibrational mode of the various isotopic permutations of CO₂ in such a way that the relative absorbances of the conveniently proximate (within 0.5 cm⁻¹) rotational lines of desirable isotopic composition are approximately equal. The ν_3 vibrational mode represents the asymmetric stretch oscillation whose resonance for CO₂ resides near the 4.37 micrometer spectral region in the infrared.

To attain this tuning, the laser was operated at various temperatures and currents around 86.04 K and 98.2 mA. For the measurement of $^{13}\text{C}/^{12}\text{C}$, the amplitude of the laser modulation current was approximately 21.1 mA to include both the P(17) "hot band" line at 2310.009 cm^{-1} for $^{12}\text{C}^{16}\text{O}_2$ and the R(40) line at 2310.348 cm^{-1} for $^{13}\text{C}^{16}\text{O}_2$. Figure 8 shows a typical scan (512 sweeps) across the spectral region containing the lines of interest.

To maximize the efficiency of the tracker, the sweep frequency was chosen such that there was approximately a 0.1 Hz beat frequency between the sweep frequency and the line-level 60 Hz signal. This was to induce slow drifts over several sweeps to bring about a condition whereby the tracker *must* track. This ensures that all tracking is taking place over *complete* cycles of any 60 Hz signals which may modulate the data (such as 60 Hz noise in the IRF).

The modulation current amplitude was fine-tuned so that the sweep time between the $^{12}\text{C}^{16}\text{O}_2$ line and the $^{13}\text{C}^{16}\text{O}_2$ line was 16.66 ms. This is required so that the lines remain in phase over the period of a 20 Hz sweep being modulated by 60 Hz noise. For example, as the sweep cycles at 20 Hz, one line is held fixed *via* the tracker but a 60 Hz frequency continues to modulate the other lines of the sweep. Thus, to ensure that the two lines being measured are in phase at 60 Hz, and assuming that one is being tracked, they must be separated by 16.66 ms in the sweep. As a standard procedure, the $^{13}\text{C}^{16}\text{O}_2$ line was tracked for all data sets.

Five separate scans, each containing 512 signal averaged sweeps for the sample, reference, evacuated, and etalon channels were taken for each CO_2 sample. The total acquisition time for five sets of 512 signal averaged sweeps for the four channels with tracking in the reference and sample channels is about twelve minutes. For some data sets, because of severe preamp noise in the evacuated beam and because of the short total acquisition time, calibration scans

from the initial evacuated scan were used with no noticeable effect on the measured isotopic ratios.

The experimental data were then analyzed using the fitting program discussed above from which the isotopic ratio of each sample could be extracted. The isotopic ratios of each of the five sets taken for each sample were averaged to give a single data point corresponding to its time during the original CO₂ gas collection.

After fitting data from the sample and reference cell, the desired isotopic enhancement of the sample cell gas relative to the reference cell gas can be obtained. For this experiment, this is

$$\left\langle \frac{\left(S_{13}/S_{12} \right)_S}{\left(S_{13}/S_{12} \right)_R} \right\rangle$$

where S₁₃ is the integrated absorbance of the R(40) ¹³C ¹⁶O₂ line, S₁₂ is the integrated absorbance of the P(17) ¹²C ¹⁶O₂ line, and the S and R subscripts represent the sample and reference channel information respectively. The angled brackets indicate that the final value was the average ratio of ratios over five separate sets.

3.3 Experimental Parameters and Assumptions

The basic assumptions of this experiment and its modeling are provided here.

The motion of carbon inside MgO was assumed to be diffusion limited. The carbon atoms are theoretically thought to hop from one O[•] site to the next after the sample temperature is changed.

Almost certainly some surface contamination is present. Any diffusional isotopic fractionation which is predicted by this model will be “diluted” by the presence of surface contamination. The process of “burning” away surface contamination was assumed to be fast and have no fractionating effects. If there are large amounts of surface contamination on the sample, the expected fractionating effect may not be observable in the data.

Moreover, it is assumed that negligible carbon isotope fractionation occurs during the reaction proposed to produce CO₂, CO, and other hydrocarbons at the surface. In addition, it is assumed that negligible carbon isotope fractionation occurs from gas handling procedures such as vacuum pumping and cryopumping.

The analytical form of the initial segregation profile $C(r,0)$ used in the diffusion model is

$$C(r,0) = N_c \left[e^{\frac{-W}{r}} + S_b \right]$$

where N_c is the number of carbon atoms at the surface, W is a characteristic width parameter, and S_b is the surface to bulk ratio. When $W=0.07$ and $S_b=0.001$, the full-width half-maximum of this profile is approximately 20 nanometers with a surface to bulk ratio of 0.001. This function was used because it qualitatively matches the profile as described by Freund.^{1,2}

The radius R of a single MgO crystal was chosen to be 100 micrometers.

A Dirichlet boundary condition at the surface ($r=R$) was chosen such that $C(R,t)=0$. This states that the concentration of carbon is always zero at the crystal surface. As soon as carbon reaches the surface while diffusing, it is instantly whisked away. This models a perfect vacuum at the surface during the experiment.

A von Neumann boundary condition at the center of the crystal ($r=0$) was chosen such that

$$\frac{\partial C(0,t)}{\partial r} = 0$$

in order to describe the condition where no material flows across the center of the crystal.

The temperature profile of the crystal as a function of time was described by a Newtonian heating curve

$$T(t) = T_f + (T_i - T_f) e^{-\gamma t}$$

The value of the characteristic heating time (γ^{-1}) was chosen to be 1000 seconds. This value is probably longer than the actual characteristic heating time of the sample. However, the results obtained by using a characteristic heating time of 1000 seconds when compared to the results obtained by using a

characteristic heating time of zero seconds will facilitate interpolation of the model data when compared to the appropriate experimental data.

An initial guess of activation energy Q was thought to be between 2.2 and 40 kJ/mole. By doing many runs using various values, $Q=30$ kJ/mole matched the experimental condition that the amount of carbon leaving the crystal at equilibrium temperature (300K) is negligible. This assumes that the ensemble of MgO crystals has created an equilibrium concentration profile of carbon after remaining at room temperature and at atmospheric pressure for several years.

The pre-exponential factor of the diffusion coefficient D_0 was varied from 10^{-11} meter²/s to 10^{-20} meter²/s giving vastly different modeling results. The measured values of D_0 and Q by H. Kathrein, H. Gonska, and F. Freund² were 2×10^{-11} meter²/s and 22.5 kJ/mole respectively. However, this result has been regarded as too fast.¹⁸ Using a value of $D_0=10^{-15}$ meter²/s gave the best match for long times to the experimental curve of CO₂ leaving the crystal per unit time as a function of time.

The rationale for using older samples of crushed MgO rather than freshly crushed samples is as follows. After the cleaving and crushing of an MgO crystal the segregation profile for a typical grain is uniform. However, over a period of three months the segregation profile is thought to become well established.¹⁹ It can then be argued that in order to ensure the steady state segregation profile for a particular temperature (like room temperature) one should wait for as long as possible until performing the measurement.

Chapter 4

Results

4.1 Modeling Results

Using the diffusion equation derived above, numerical results were generated. Once the parameters were estimated, model data representing the isotopic ratio as a function of time were generated and compared to experimental data representing the isotopic ratio as a function of time.

Note that for the purposes of modeling, the isotopic enhancement of $^{13}\text{C}/^{12}\text{C}$ is compared to the initial ^{13}C and ^{12}C amounts in the crystal samples. Thus, the absolute numbers generated by the model may be incorrect for any given crystal since the standard may be different. That is, the reference gas for the experimental data and the "reference gas" for the model data are different, thus introducing an offset to the compared data sets. However, the magnitude of the variations for a given set of parameters for model data is comparable to experimental data.

Figure 9 shows the modeled isotopic ratio as a function of time for the cases of instant and non-instant heating using values of $D_0=10^{-15}$ meter²/s and $Q=30$ kJ/mol for the pre-exponential factor and the activation energy. This is using a standard segregation profile of full-width half-maximum of 20 nanometers and bulk to surface ratio of 0.001. Figure 10 shows the modeled

concentration of carbon diffusing in the crystal plotted every 1000 seconds. For the case of instant heating, a value of 700K was used as the temperature. For the case of non-instant heating, a value of 1000 seconds was used as the characteristic heating time, a value of 700K was used for the bath temperature, and a value of 300K was used for the initial temperature. Figure 11 shows the carbon leaving the crystal during each timestep as a function of time for the cases of instant and non-instant heating. The total modeled diffusion time should occur over experimental time scales, so a value of 10^4 seconds (167 minutes) was chosen. Since the largest allowed time step has already been determined by the stability criterion, this also fixes the maximum number of time steps allowed. For the above analysis the total number of time steps used was 2420. To be conservative, this value was generated using a time step half that required by stability.

For comparison, Figure 12 shows the modeled isotopic ratio as a function of time using the same set of parameters as above except with a constant segregation profile (no enthalpy of segregation) for the cases of instant and non-instant heating. Figure 13 shows the modeled concentration of carbon diffusing in the MgO lattice with a constant potential. Finally, Figure 14 shows the carbon coming out of the crystal during each timestep as a function of time for the cases of instant and non-instant heating with a constant potential.

By comparing Figure 14 and its experimental data counterparts Figure 15 and Figure 17, it can be seen that an instant heating profile model is insufficient to properly model this data (note that the scales in these figures are not absolute). Again from Figure 14 it can be seen that the non-instant heating profile better emulates the experimental data. This can be seen by noting the sharp increase in CO_2 gas per unit time with a maximum occurring around 30 minutes for the model data. In the experimental data of Figures 15 and 17 the

maximum occurs at 4 minutes and 9 minutes respectively. The discrepancy between the two experimental peak locations is due to the different heating temperatures of the two samples. The difference in modeled peak location and experimental peak location is due to the choice of γ^{-1} in generating the modeled data. Finally, just as in the experimental data, the model data then taper off towards zero as the gas in the crystal is depleted.

4.2 Data Results

The experiment was performed on three separate MgO samples named sequence one, sequence two, and sequence three. Each sample contained a different amount of MgO and was heated to a slightly different temperature (all around 400°C). The points in the plots of the isotopic ratios are all averages of five sets of scans as described in section 3.2.

Sequence one data represent CO₂ gas evolved from 15 grams of MgO powder heated to a temperature of approximately 377°C. Figure 15 shows the amount of CO₂ coming out of the crystals per unit time as a function of time. Figure 16 shows the relative isotopic enhancement of ¹³C/¹²C as compared to the standard laboratory CO₂ tank gas.

Similarly, sequence two data are from CO₂ gas degassing from 7.5 grams of MgO at 400°C. Figure 17 shows the CO₂ degassed per unit time as a function of time. Figure 18 shows the relative isotopic enhancement of sequence two data relative to laboratory tank gas.

Sequence three data were taken near 400°C with approximately 5 grams of MgO. Figure 19 shows the relative isotopic enhancement relative to

laboratory tank gas. Note, that the exact time scale of sequence three was not recorded and only the relative chronological order of the data points is known.

The scatter of the five scans about their average for each data point were typically well below $\pm 0.1\%$. However, the errors in the data were not limited by precision, but by the accuracy of the instrument. If all the data from all sequences are taken together as a horizontal line, as illustrated by the scatter plot in Figure 20, the standard deviation is $\pm 0.125\%$. The previously known accuracy of the SILS instrument was $\pm 0.2\%$.³ Thus, the data demonstrate a significant improvement in the last reported accuracy of the SILS.

Chapter 5

Discussion

An isotopic enhancement as great as 4% was expected if carbon atoms were diffusing through the MgO lattice and forming CO₂ at the surface.²⁰ The numerical results have confirmed this expected isotopic enhancement. However, the experimental data are constant within the estimated instrumental error of $\pm 0.125\%$, implying there is no isotopic fractionation. Previous attempts at extracting information about the isotopic fractionation of carbon dioxide degassing from MgO essentially resulted in data which contained characteristic diffusion fractionation data just outside the estimated noise. With this improved diffusion model and the improved instrument, a similar result can be seen for sequence one, two, and three data in the carbon ratios. However, since evidence for fractionation had previously been observed just outside the noise when the accuracy of the instrument was $\pm 0.4\%$ ^{6,13} and the current evidence for fractionation appears to be just within the noise for $\pm 0.2\%$ accuracy, this would lead one to the conclusion that indeed no time-dependent fractionation exists for the data. In fact, these data, taken as a constant, redefine the instrumental accuracy at $\pm 0.125\%$.

However, several complications must be addressed before drawing a final conclusion regarding the presence of solute C in MgO. For example, if significant CO is also involved in the degassing process, as is predicted, then

fractionation may occur during that chemical reaction at the surface of the crystal. This may seem unlikely, but since isotopic ratios in CO were not measured, this information is not available.

A more important observation addresses both the age of the sample and the manner in which it was stored.¹⁹ Until recently it had been assumed that the delay time from the moment of cleaving and crushing of the crystal to the moment of heating would have an interesting but non-catastrophic effect on the measurement of time dependent isotope fractionation.

Upon more critical analysis, it has become clear that early assumptions which were made about the time scales over which samples reached steady state may have been incorrect. Earlier it was argued that older samples would contain a segregation profile which had reached a steady state. Using this argument, samples five years old were used. However, it is now believed that five years is far longer than the time it takes for the sample to reach a steady state profile. If too much time elapses between the reaching of a steady state profile and performing the desired measurement on the sample, the segregated carbon begins undergoing complicated chemistry at the surface, becoming indistinguishable from surface contamination.

Because of the introduction of this surface chemistry, fresher samples must be used and a more rigorous process of sample preparation and storage must be implemented. Freshly crushed MgO samples which will have negligible surface contamination and surface chemistry¹⁹ are being prepared for the purposes of repeating this experiment under identical experimental conditions. Experiments will be performed using samples of different ages after crushing (*e.g.*, one month, two months, three months, *etc.*). This will permit the measurement and modeling of solute C in MgO undergoing the development of a segregation profile. By performing many of these experiments over many

months, the amount of time required to reach a steady state can be determined. The ages of the samples used for this thesis are very old compared to the ages of the samples in the proposed experiment above. Thus the data in this thesis will provide a standard for the long term effects of sample age on isotopic fractionation.

The current means of acquiring data, although demonstratively accurate, are tedious and inefficient. Experimental logistics could be greatly enhanced by the addition of a flow system, as suggested by Trice.⁶ With electronically controlled needle-valves to hold the pressure in the sample cell constant, real-time MgO heating and CO₂ data acquisition could be implemented. Very early times (< 1 minute) and very late times (> 300 minutes) could then be carefully mapped out in this fashion.

In addition to improvements in experimental logistics, there are several improvements which could be made to the diffusion model. In general, for a model to correctly predict data, one must have a reasonable grasp of the values of the parameters. In the case of this diffusion model, several experiments would fix the three important parameters.

To measure the characteristic heating time γ^{-1} of MgO in a glass flask emerged in a molten metal bath, a thermocouple could be placed inside the MgO power as it is heated. The temperature could then be measured as a function of time, recorded, and then used as the heating profile $T(t)$ in the diffusion model.

Furthermore, the measurement of CO₂ gas evolving from MgO could be done at many temperatures spanning several hundred degrees. The total carbon per unit time leaving the crystal as a function of time would give information about the pre-exponential factor D_0 and the activation energy Q . This could be done by comparing experimental data to values generated from the model and finding a best fit for some set of model parameters. Experiments exactly of this

nature, designed to measure other properties of CO₂ produced by heating MgO, have already been performed. However, preliminary data give unreasonable results for the values of D₀ and Q. Further evaluation is required before confidently incorporating their results into this model.

Because of the stringent computational limitations on the model imposed by the stability criterion and by computer speed, a better space and time-axis resolution scheme could be implemented. It has been pointed out²¹ that a straightforward relationship between a potential near a boundary and a mixed von Neumann/Dirichlet boundary condition may exist. When such a relationship is produced, it will allow the transformation of the diffusion equation with a surface associated potential having a zero boundary condition at the edge of the crystal, to a simple spherical diffusion equation with no surface potential and a mixed boundary condition. This will allow, after dynamic equilibrium is achieved near the boundary, relaxation of the space resolution which will allow relaxation of the stability criterion and time resolution. Consequently, longer modeled diffusion times will be achieved. In turn, for early times, this improved technique will facilitate highly increased resolution of the grid points to eliminate the possibility of any early transient numerical artifacts.

Also there are other numerical techniques which are potentially more accurate and unconditionally stable. Crank-Nicholson^{11,12} is an example of one such model. This implicit numerical technique is second order accurate in time but generally requires the inversion of a large matrix which can consume considerable computer time.

Additionally, efforts are being made to improve the SILS instrument. The present laser current driver is known to have an approximately non-Gaussian noise profile due mainly to 60 Hz line noise in the driver circuitry. However, the modeling of the current noise assumes its profile to be Gaussian. Even with a

tracker (which minimizes the non-Gaussian noise), this disallows the complete removal of the effects of the current noise. A new current driver for the SILS instrument is scheduled to replace the present one which will hopefully render the noise profile more Gaussian and thus easier to model.

The significant improvement in the accuracy of the instrument as determined by this data addresses an important issue regarding the sensitivity of the data acquisition technique to varying experimental conditions. These data were taken over many days through many gas handling phases and over a variety of laser operating conditions. Yet the instrument was still able to measure accurate data. This indicates that the experimental technique is sound and free of fractionation inducing effects.

Chapter 6

Conclusion

Though the data suggest that no isotopic fractionation of carbon in carbon dioxide is taking place during the heating of magnesium oxide, there are some issues which deem further investigation before drawing a final conclusion regarding the presence of solute C in MgO. The method of data acquisition can be deemed sound by observing that these data have set the accuracy of the SILS instrument at $\pm 0.125\%$; this is a reasonable improvement over the previously established value of $\pm 0.2\%$. However, some surface chemistry has been hypothesized to have occurred which upon heating generated CO_2 from the crystal which was indistinguishable from surface contamination; this was probably due to over aging the sample. It was originally thought that the extra time between crushing and measuring the sample would improve the chances of measuring a sample which had reached steady state. However, other long term effects seem to have degraded the sample. Thus the data presented herein alone are insufficient to confirm or deny the presence of solute C in MgO. However, these data may provide a standard for future experiments, indicating the long term effects of sample age on the isotopic fractionation of carbon in carbon dioxide during heating. The experiment will have to be repeated using highly purified and carefully prepared MgO powder.

In addition, the lack of early time and late time data removes the possibility of seeing a broader picture. The introduction of a gas flow system technique, though introducing its own set of subtle issues in measurement, can address these issues. The accurate modeling of very early times and very long times will greatly enhance the predictive capabilities of the diffusion model. This will occur such that entire experiments can be modeled over experimental time lengths with confidence in the numerical output.

Finally, the ability to fix the values of the parameters in the model will also greatly enhance its predictive abilities. By eliminating the uncertainty in basic parameters such as the diffusion coefficient and the heating rate, emphasis can be placed upon modeling different experiments rather than isolating the values of several parameters. This could be done by a series of experiments as described in Chapter 5.

Because of the subtleties involved in properly performing this challenging experiment, the avenues of measurement and improvement, as described above, should be explored before concluding that no solute C is present in MgO.

Chapter 7

Figures

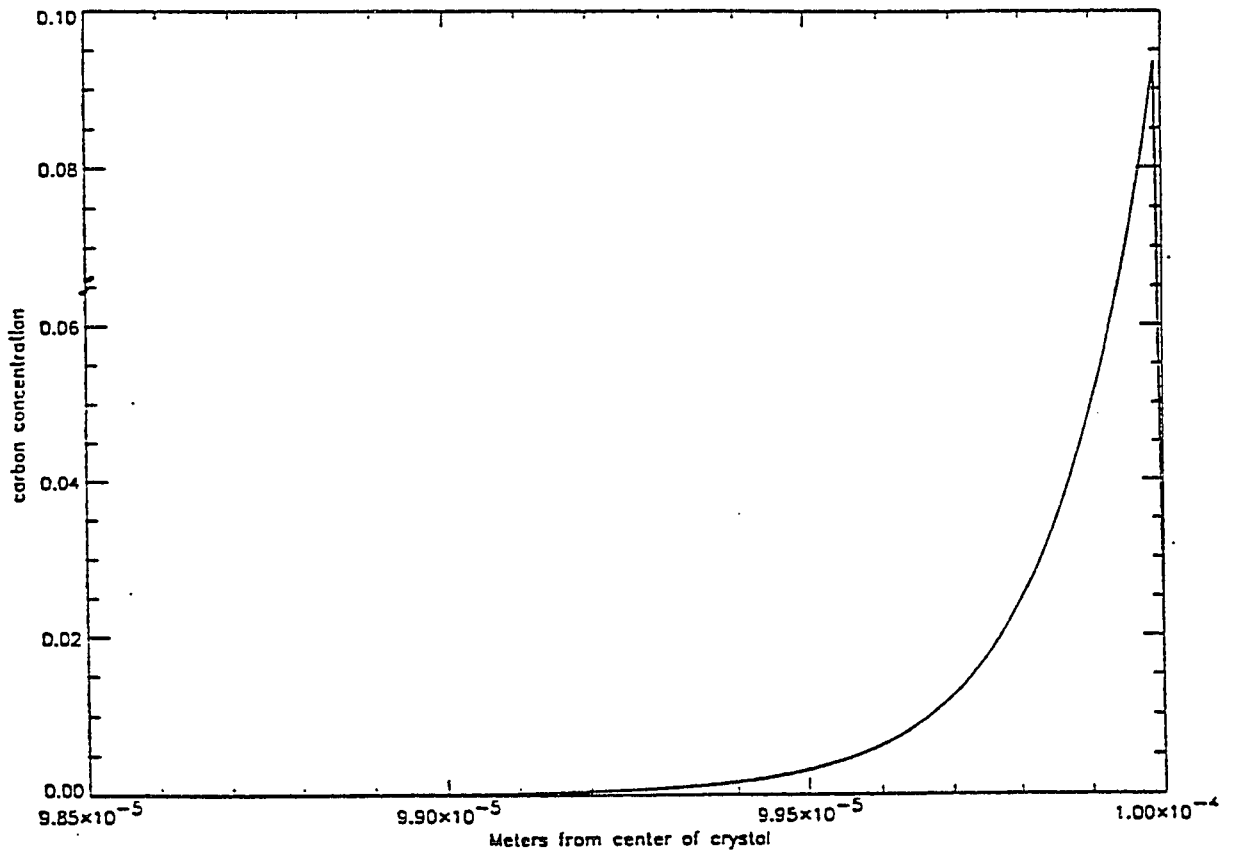


Figure 1: Theoretical segregation profile of carbon in a MgO crystal of radius 100 micrometers.

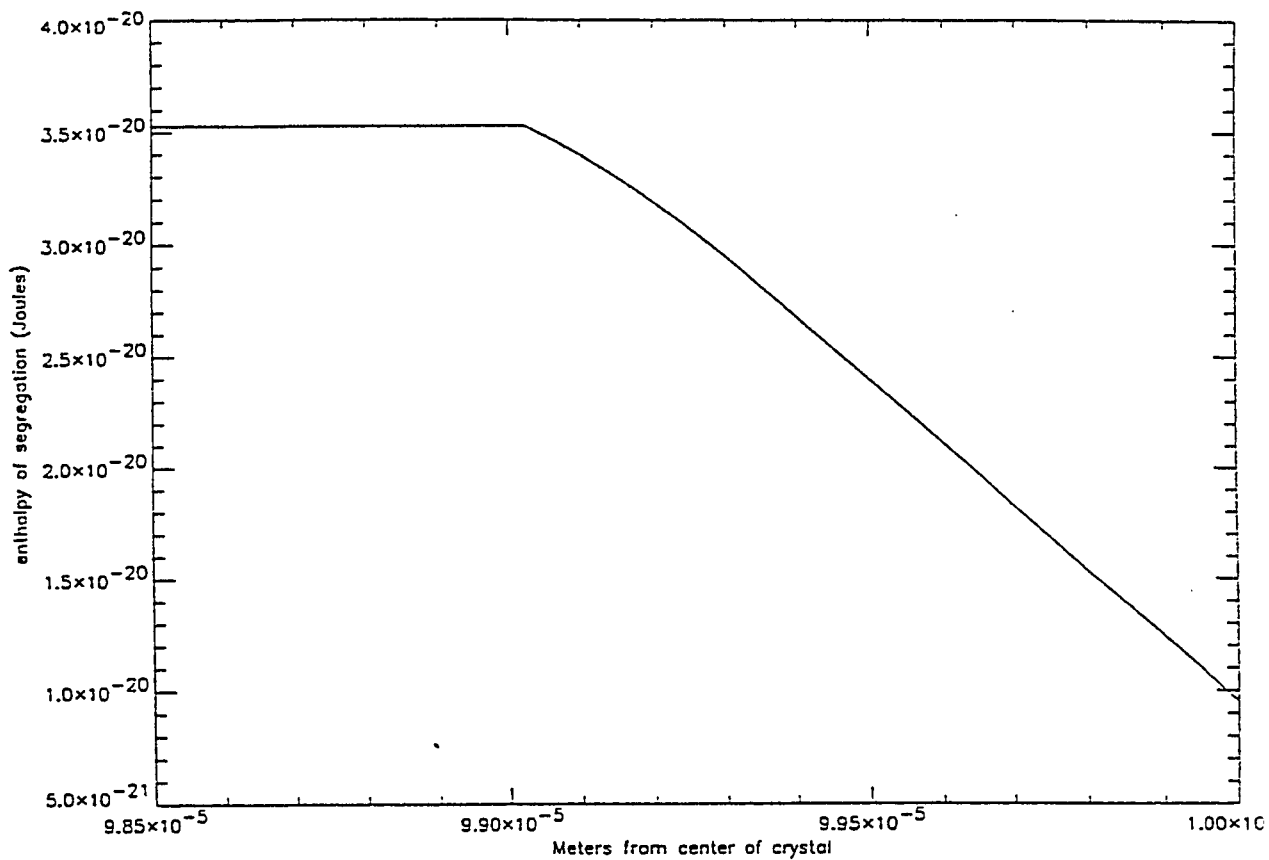


Figure 2: The enthalpy of segregation for the segregation profile in Figure 1.

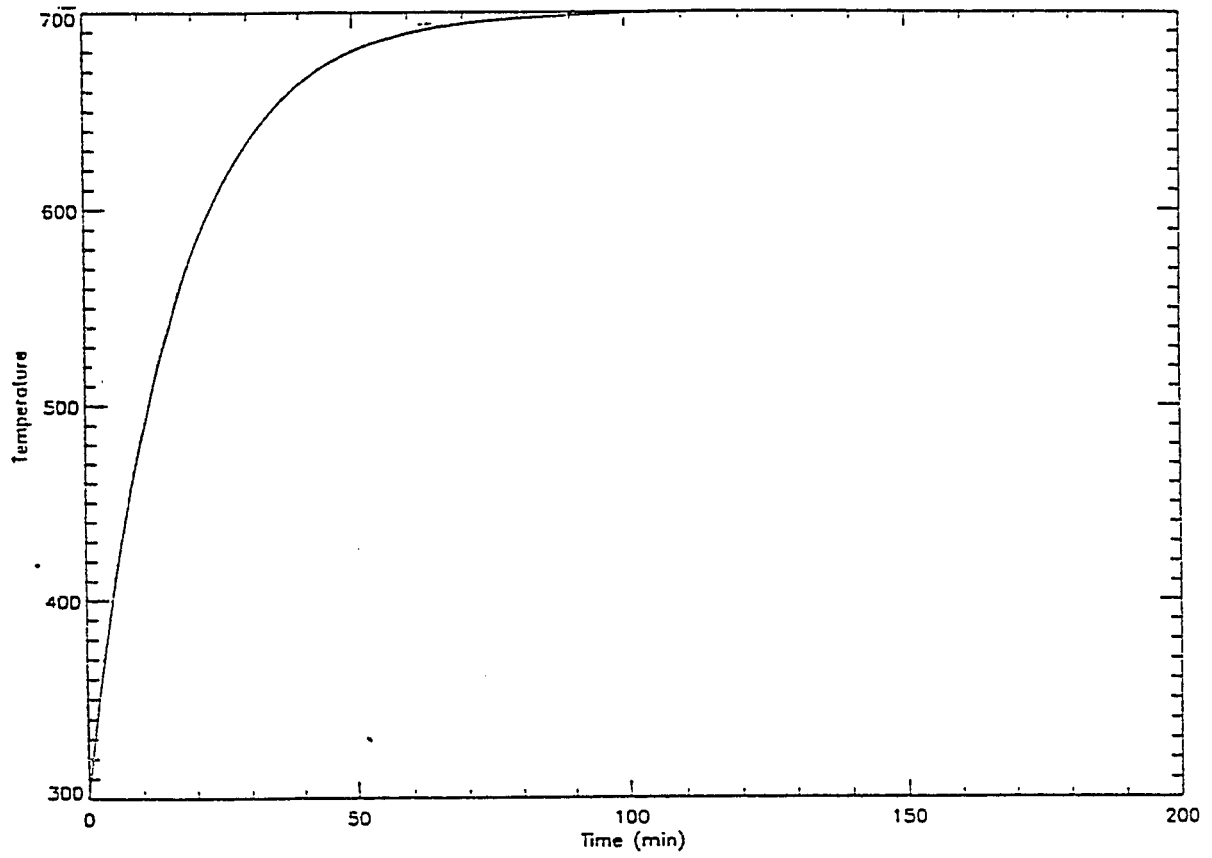


Figure 3: A Newtonian heating profile with a characteristic heating time of 1000 seconds.

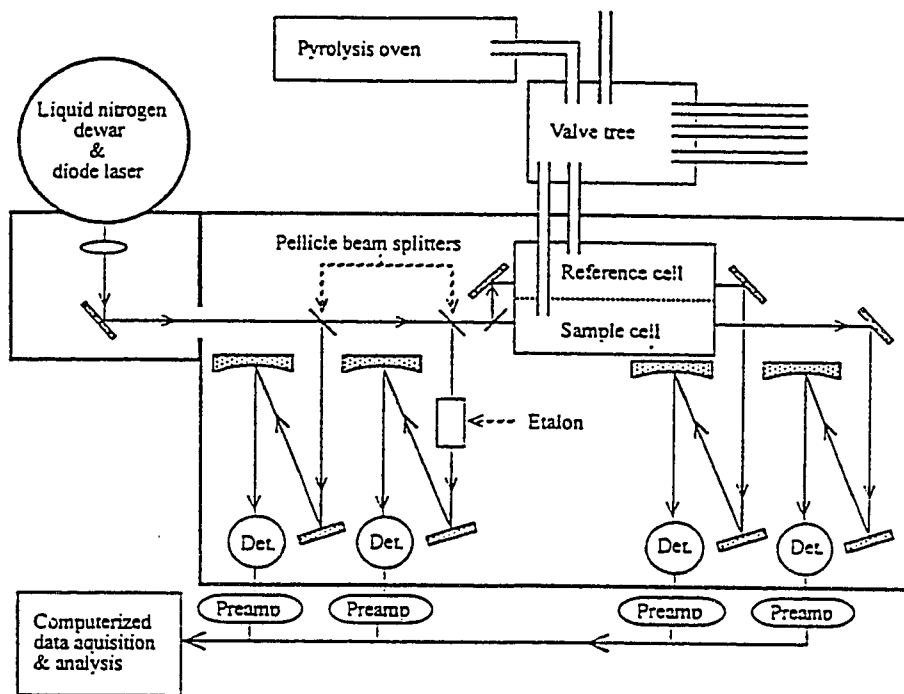


Figure 4: A schematic of the SILS instrument.

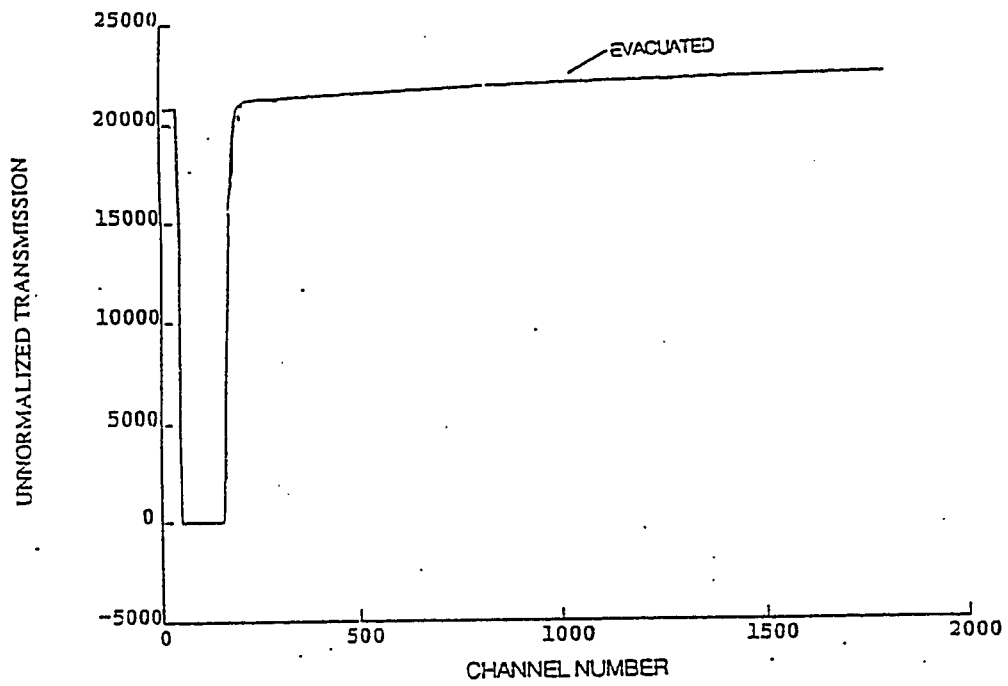


Figure 5: A typical evacuated scan with a blanking pulse. In this figure, the channel number is proportional to the output frequency of the laser.

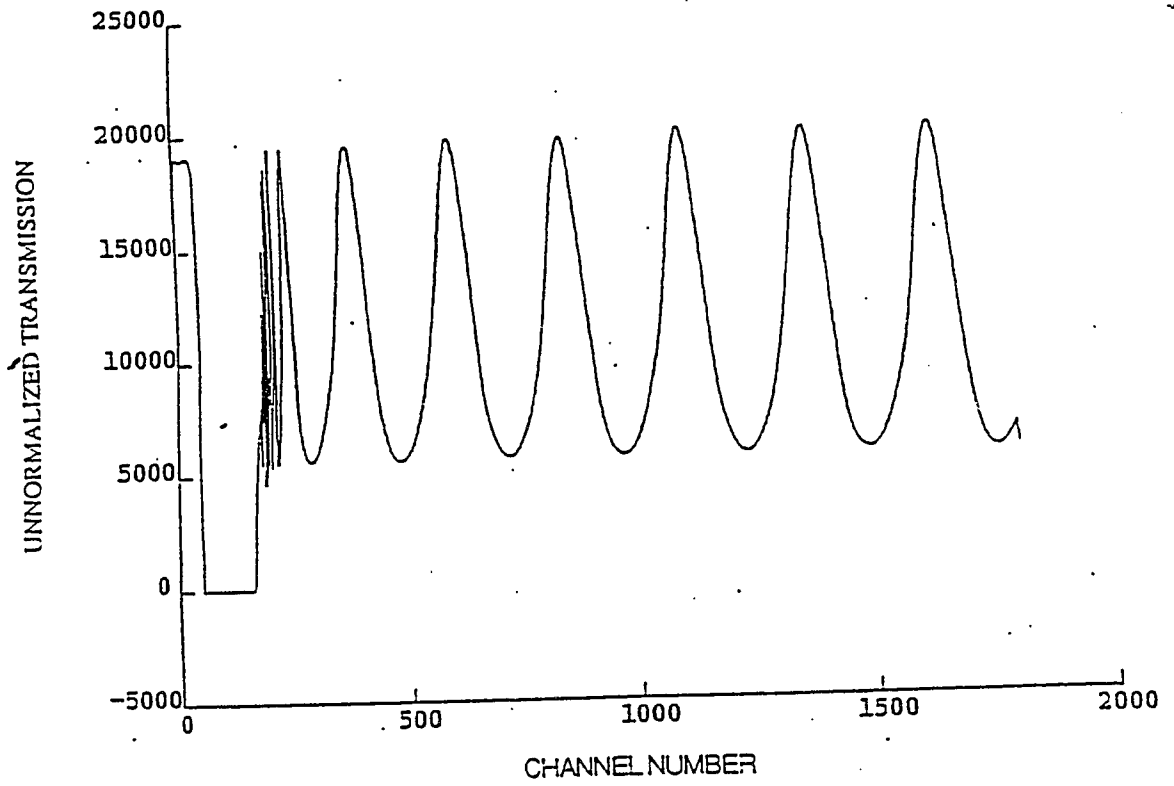


Figure 6: A typical etalon scan with a blanking pulse. In this figure, the channel number is proportional to the output frequency of the laser.

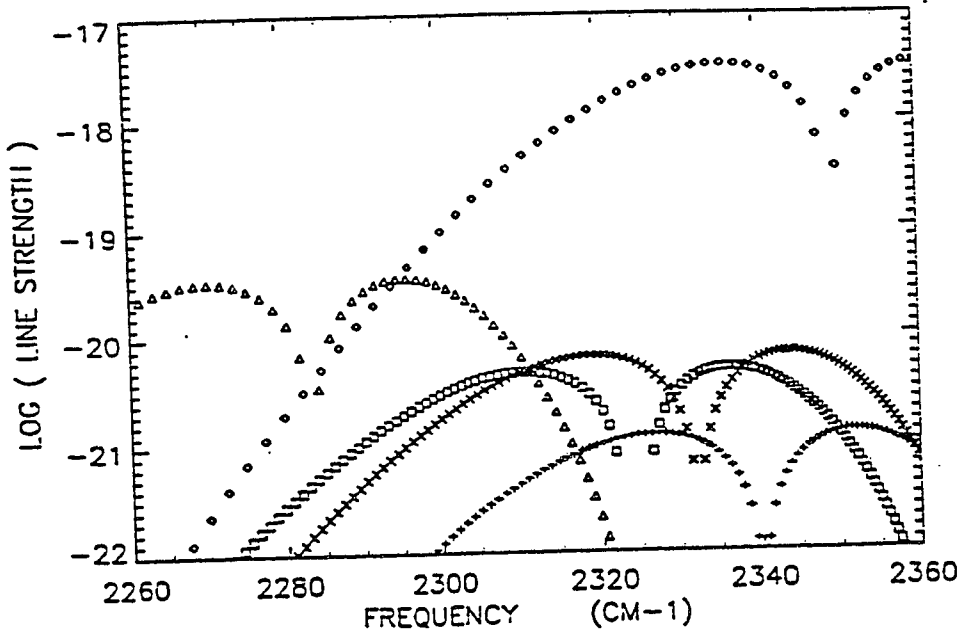


Figure 7: A schematic of some CO₂ absorbance bands in the 2310 cm⁻¹ region.

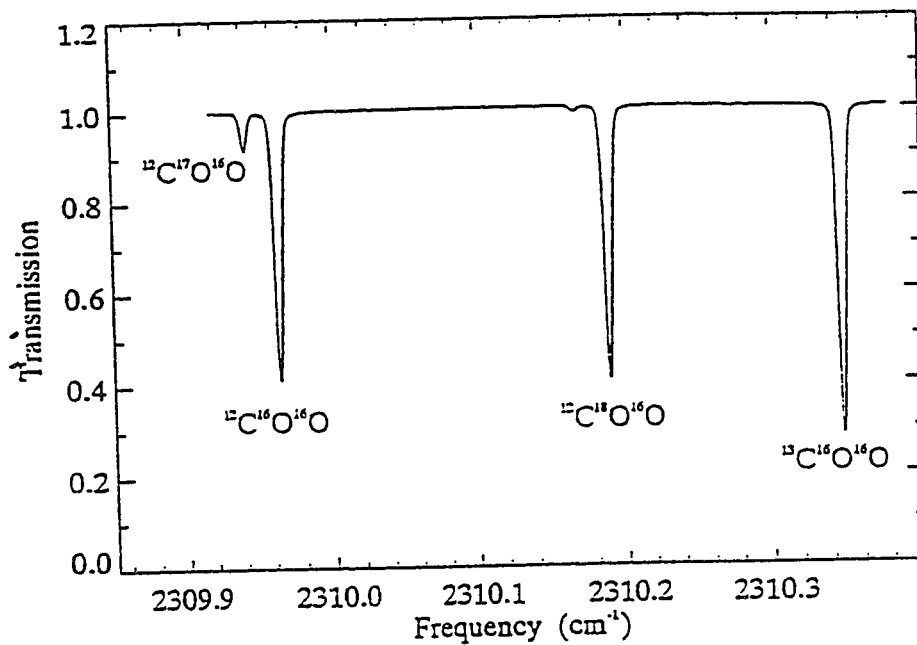


Figure 8: Transmission as a function of wavenumber for a scan across the spectral lines of interest. In particular P(17) ($^{12}\text{C}^{16}\text{O}^{16}\text{O}$) near 2309.96 cm^{-1} and R(40) ($^{13}\text{C}^{16}\text{O}^{16}\text{O}$) near 2310.34 cm^{-1} are the lines used to measure the relative isotopic enhancement of $^{13}\text{C}/^{12}\text{C}$.

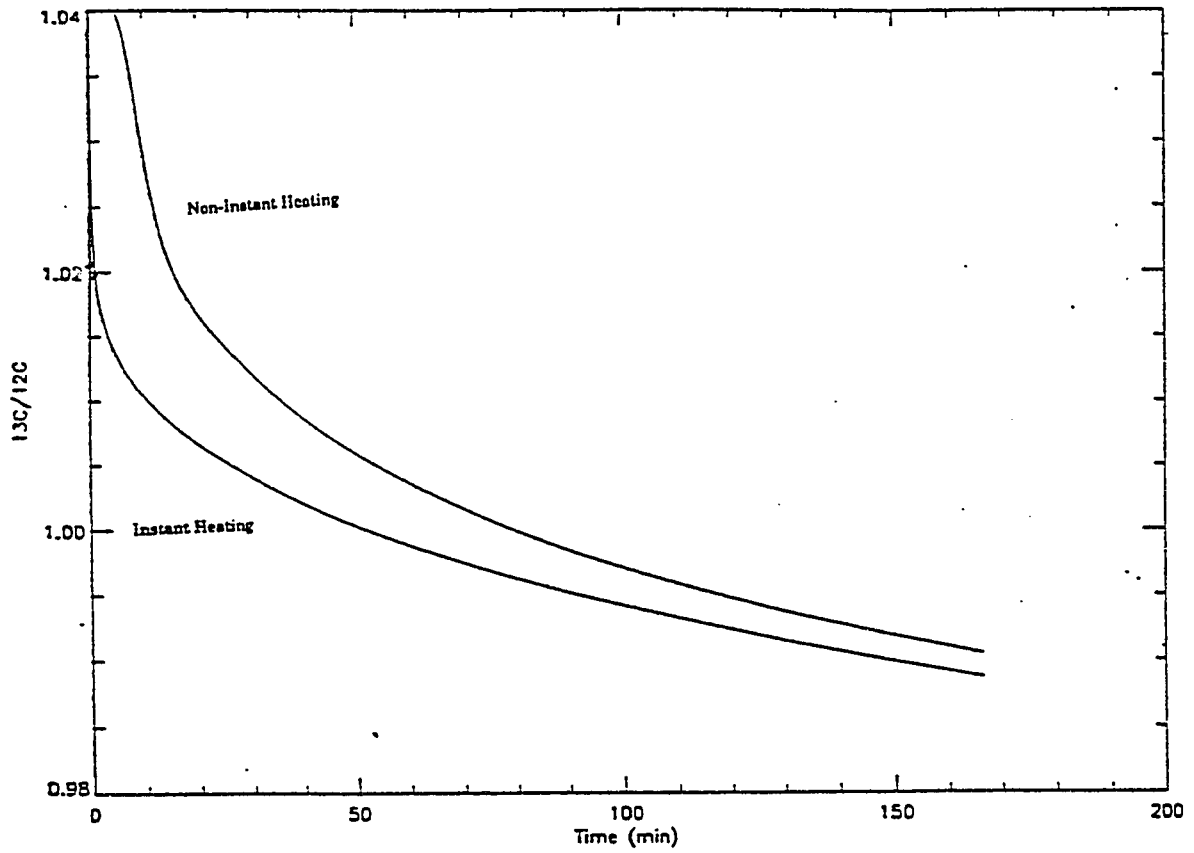


Figure 9: Plots for the cases of instant and non-instant heating for a modeled $^{13}\text{C}/^{12}\text{C}$ ratio as a function of time resulting from diffusion in the potential from Figure 2. For the non-instant heating case, the temperature profile is the same as in Figure 3.

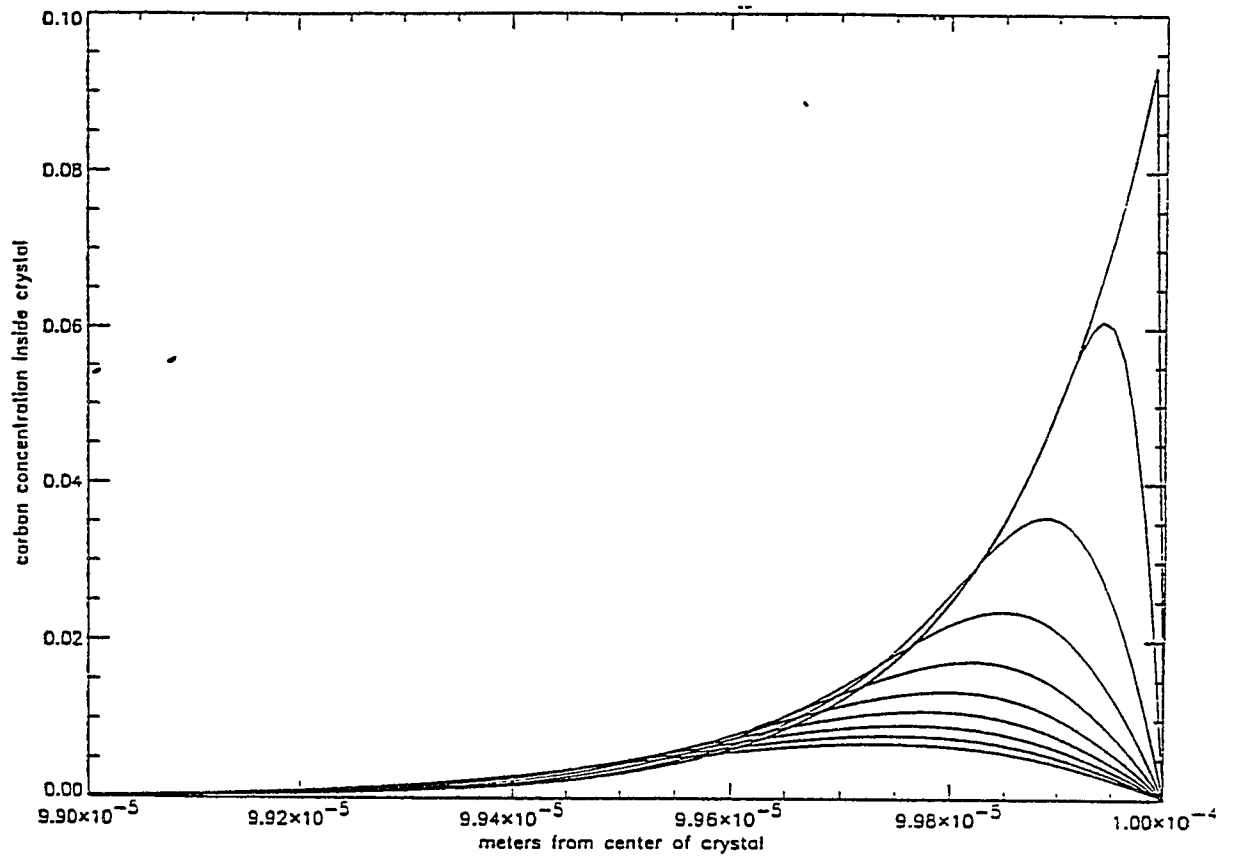


Figure 10: Ten plots of the modeled carbon profile inside MgO plotted for 1000 second intervals for a total of 10000 seconds resulting from diffusion in the potential from Figure 2. The heating profile is the same as in Figure 3.

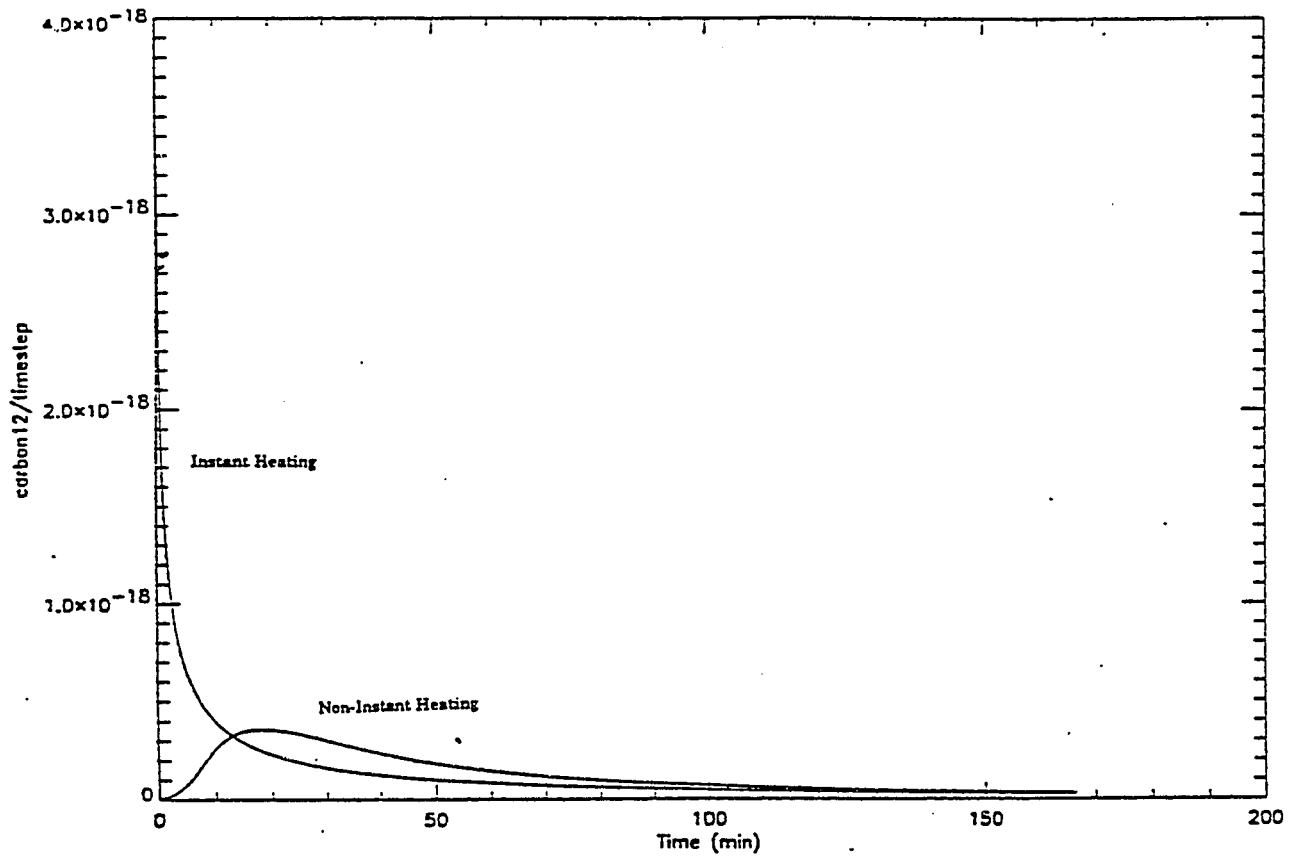


Figure 11: Plots for the cases of instant and non-instant heating for modeled carbon leaving the crystal per unit time as a function of time resulting from diffusion in the potential from Figure 2. For the non-instant heating case, the temperature profile is the same as in Figure 3.

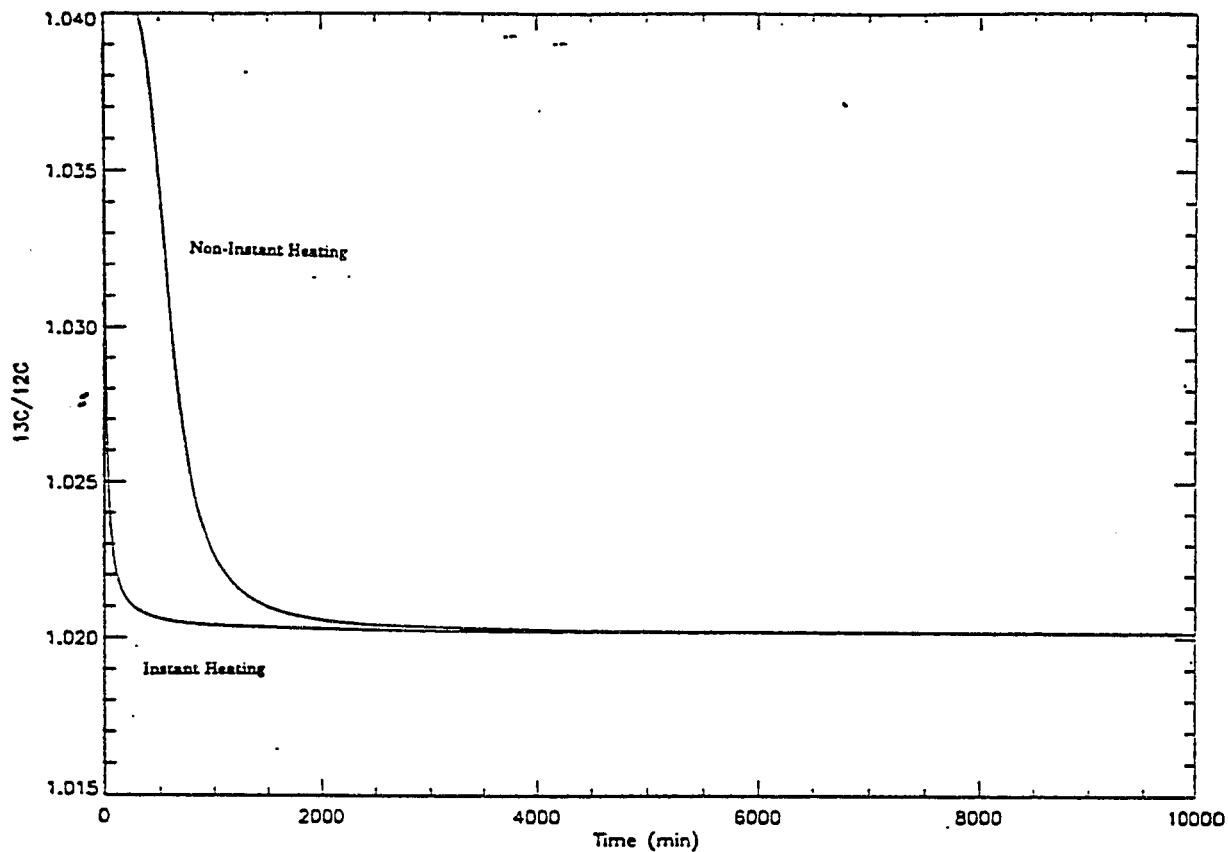


Figure 12: Plots for the cases of instant and non-instant heating for a modeled $^{13}\text{C}/^{12}\text{C}$ ratio as a function of time resulting from diffusion in a constant potential. For the non-instant heating case, the temperature profile is the same as in Figure 3.

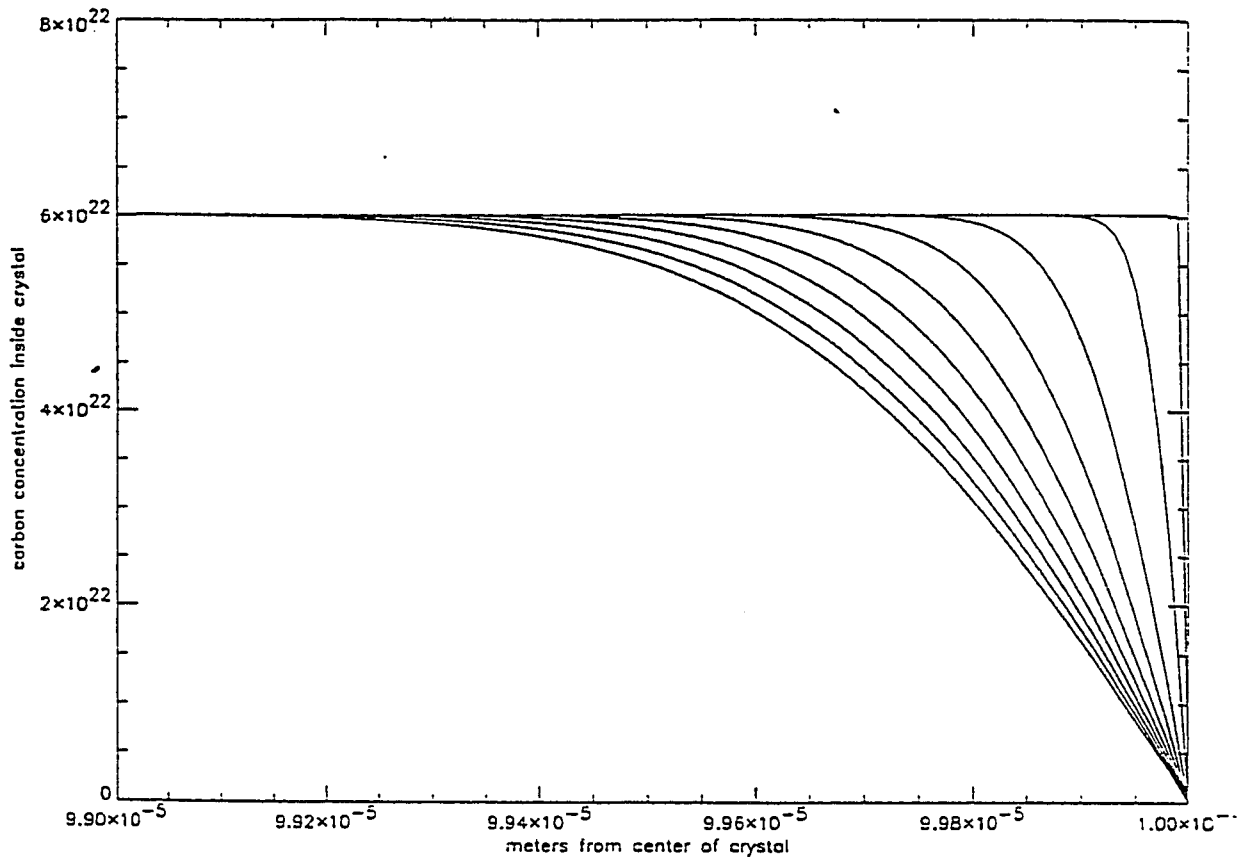


Figure 13: Ten plots of the modeled carbon profile inside MgO plotted for 1000 second intervals for a total of 10000 seconds resulting from diffusion in a constant potential. The heating profile is the same as in Figure 3.

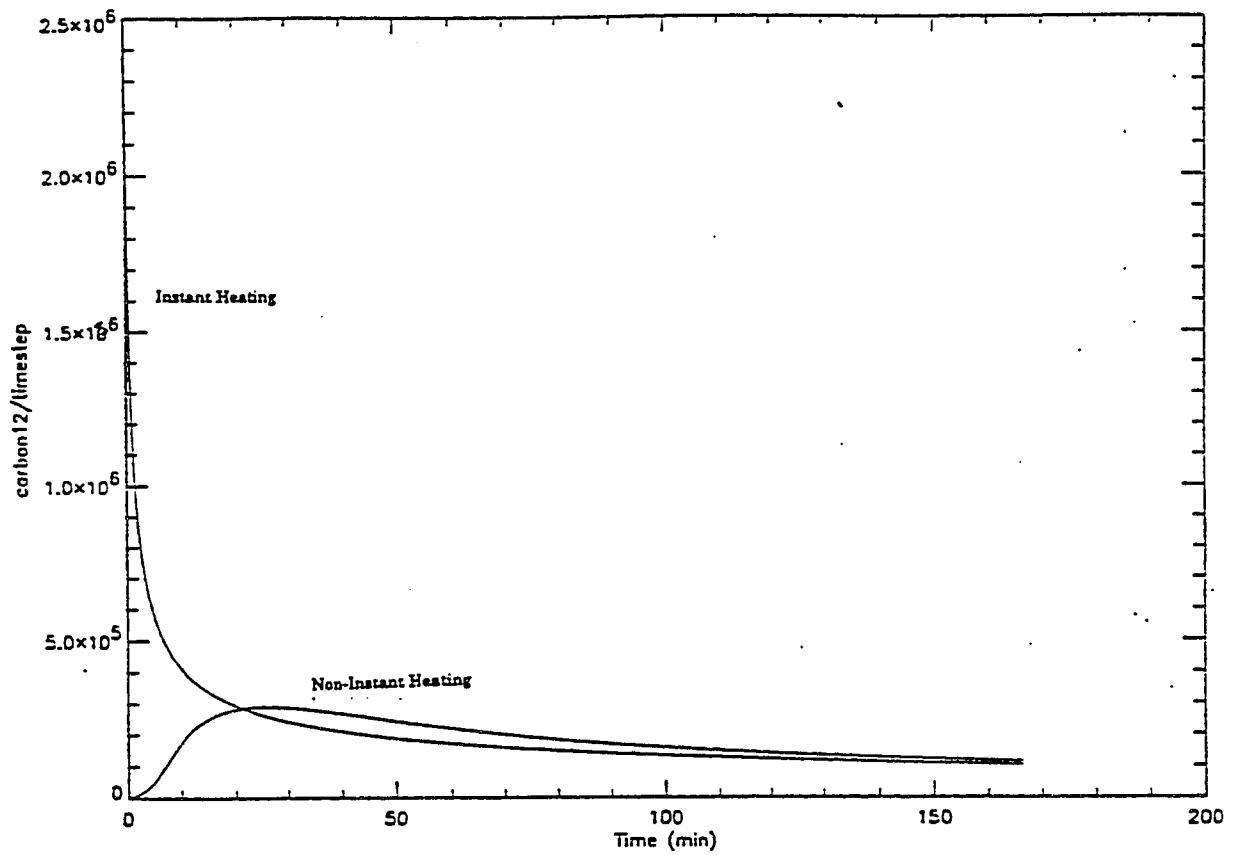


Figure 14: Plots for the cases of instant and non-instant heating for modeled carbon leaving the crystal per unit time as a function of time resulting from diffusion in a constant potential. For the non-instant heating case, the temperature profile is the same as in Figure 3.

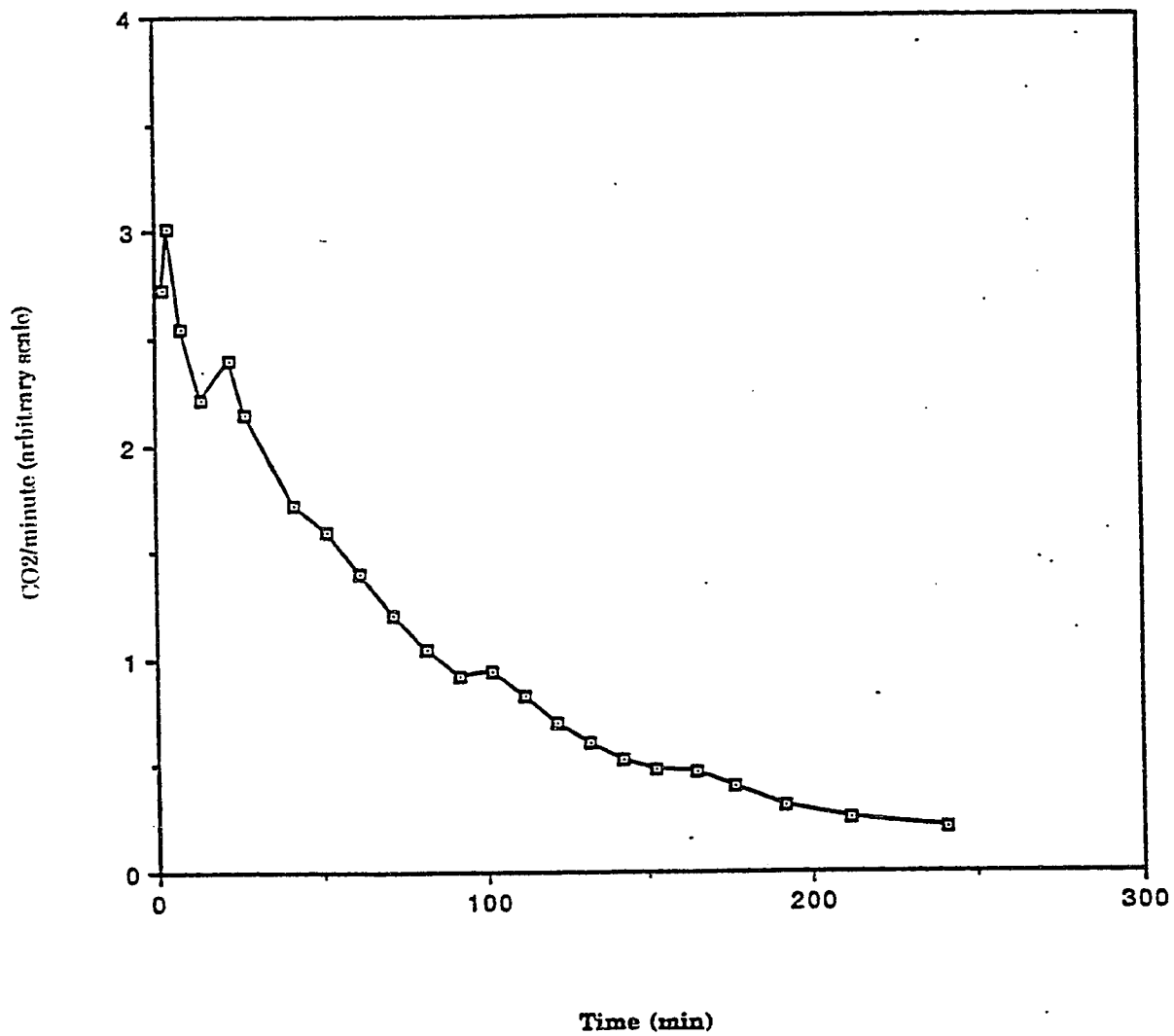


Figure 15: Carbon dioxide leaving the crystal per unit time as a function of time for sequence one data (15 grams of MgO heated to 377°C).

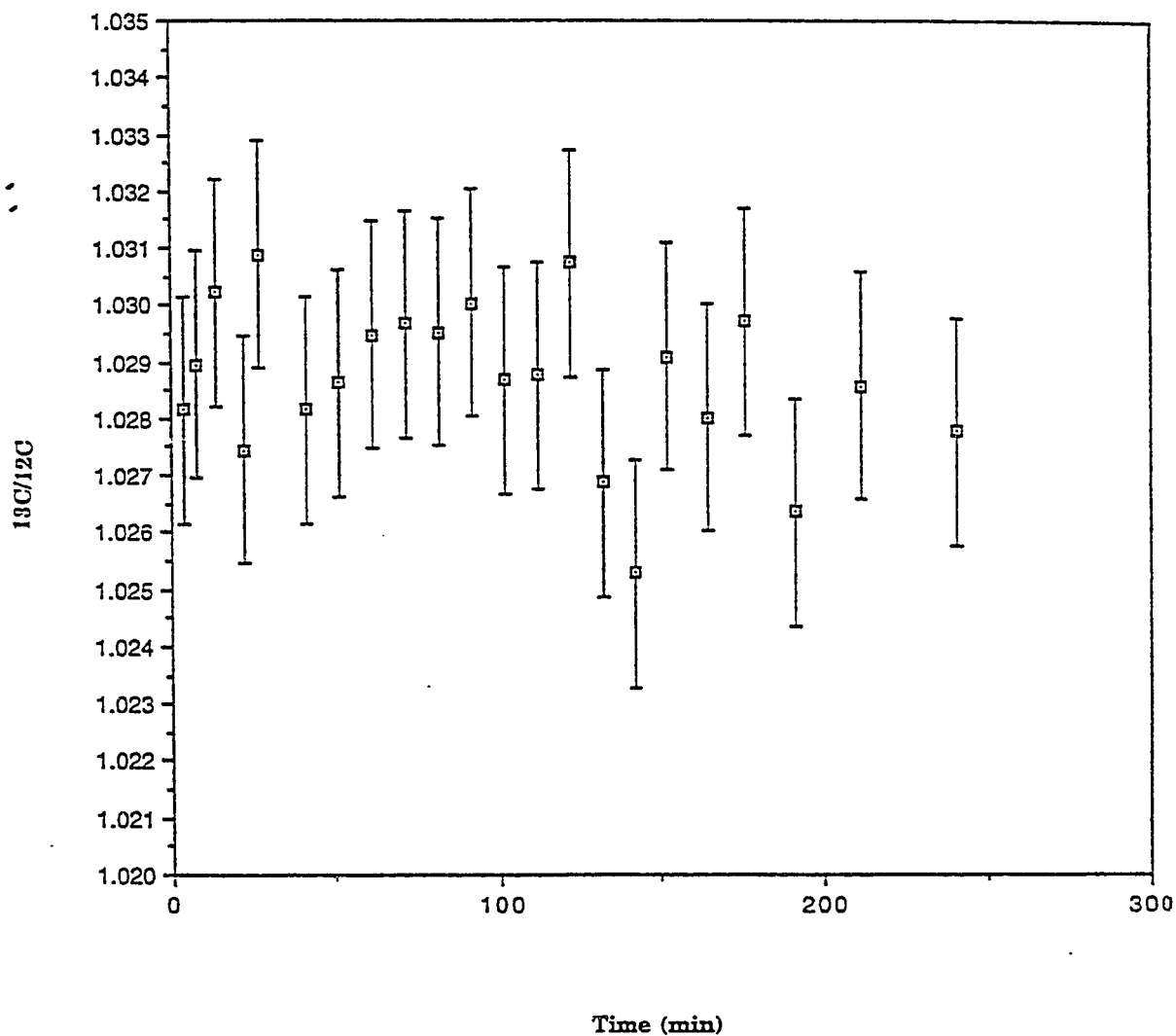


Figure 16: $^{13}\text{C}/^{12}\text{C}$ ratio as a function of time for sequence one data (15 grams of MgO heated to 377°C). Each data point is the average of five separate scans of 512 sweeps each. The error bars indicate the known accuracy of the SILS instrument of 0.2%.³

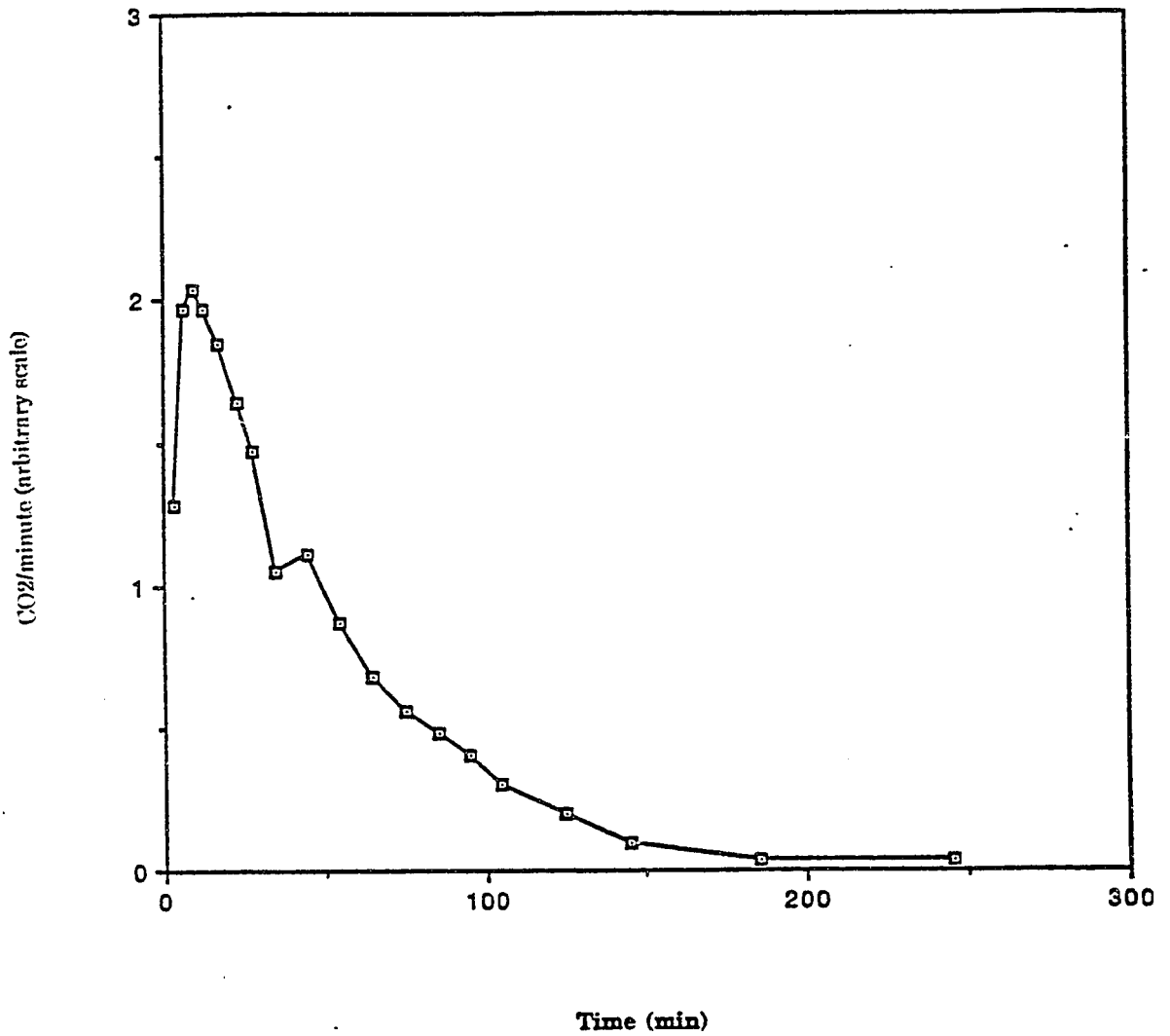


Figure 17: Carbon dioxide leaving the crystal per unit time as a function of time for sequence two data (7.5 grams of MgO heated to 400°C).

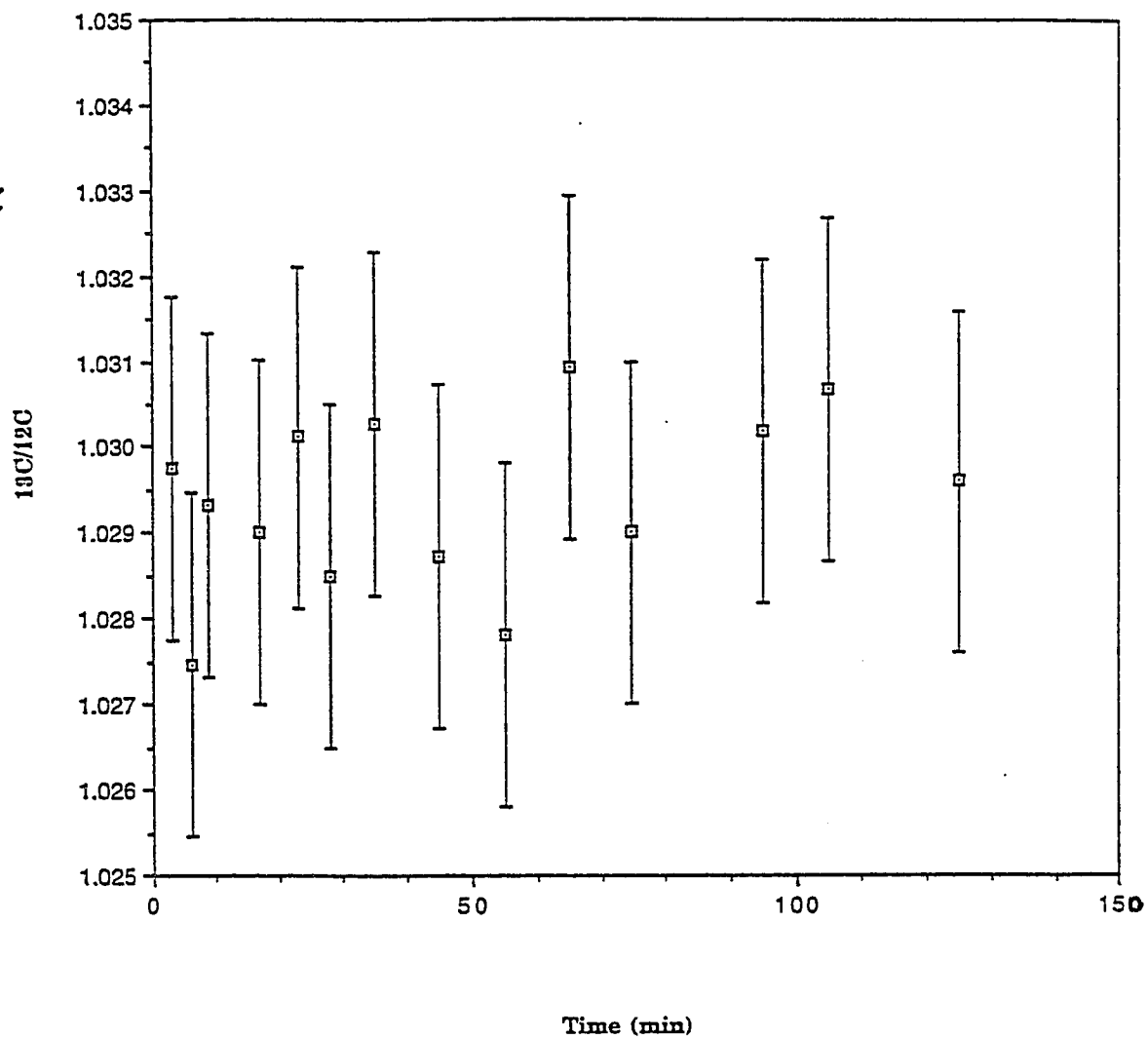


Figure 18: $^{13}\text{C}/^{12}\text{C}$ ratio as a function of time for sequence two data (7.5 grams of MgO heated to 400°C). Each data point is the average of five separate scans of 512 sweeps each. The error bars indicate the known accuracy of the SILS instrument of 0.2%.³

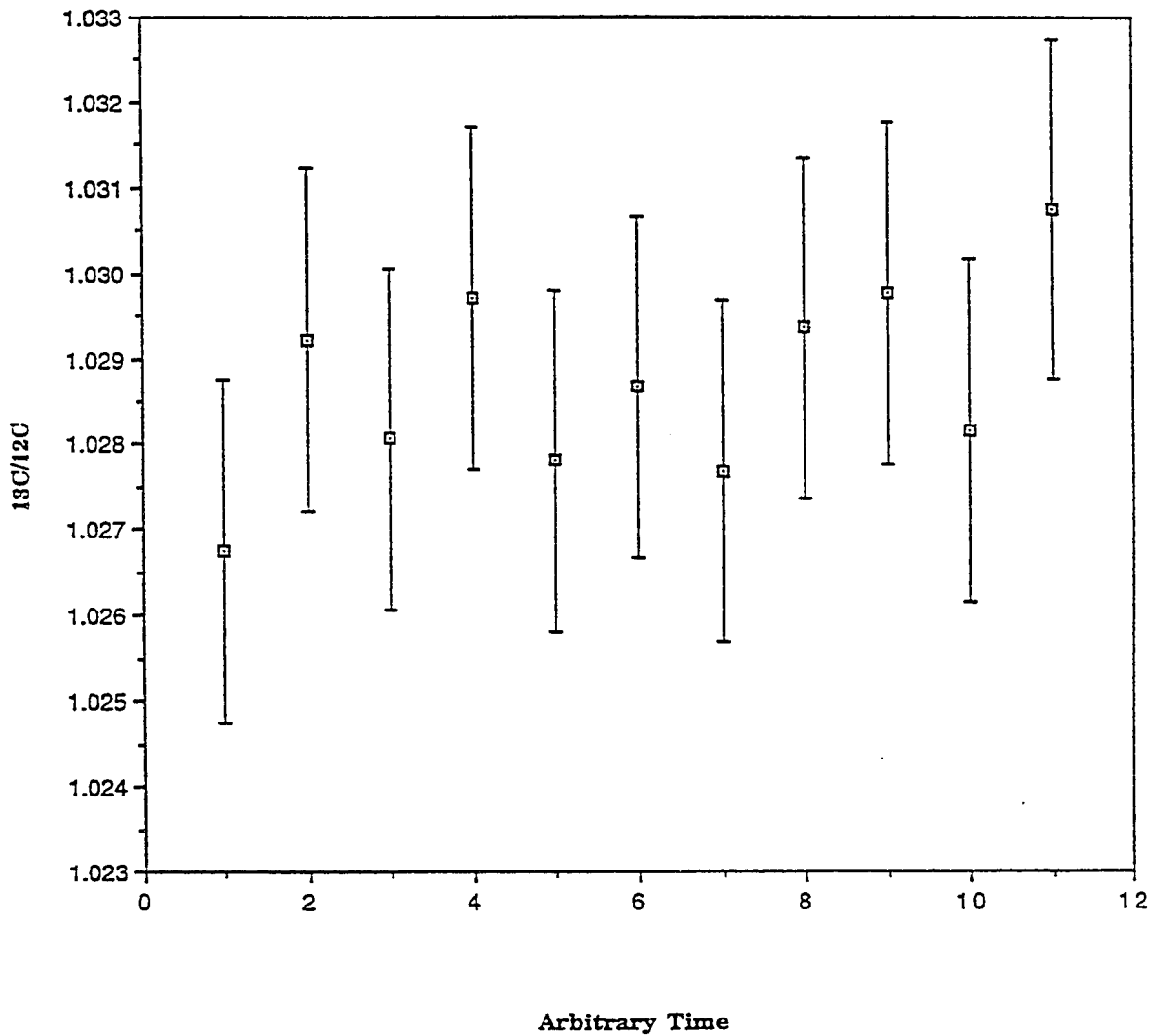


Figure 19: $^{13}\text{C}/^{12}\text{C}$ ratio as a function of time for sequence three data. Note the time axis is chronological but arbitrary in spacing, since no time information was available for sequence three data. Each data point is the average of five separate scans of 512 sweeps each. The error bars indicate the known accuracy of the SILS instrument of 0.2%.³

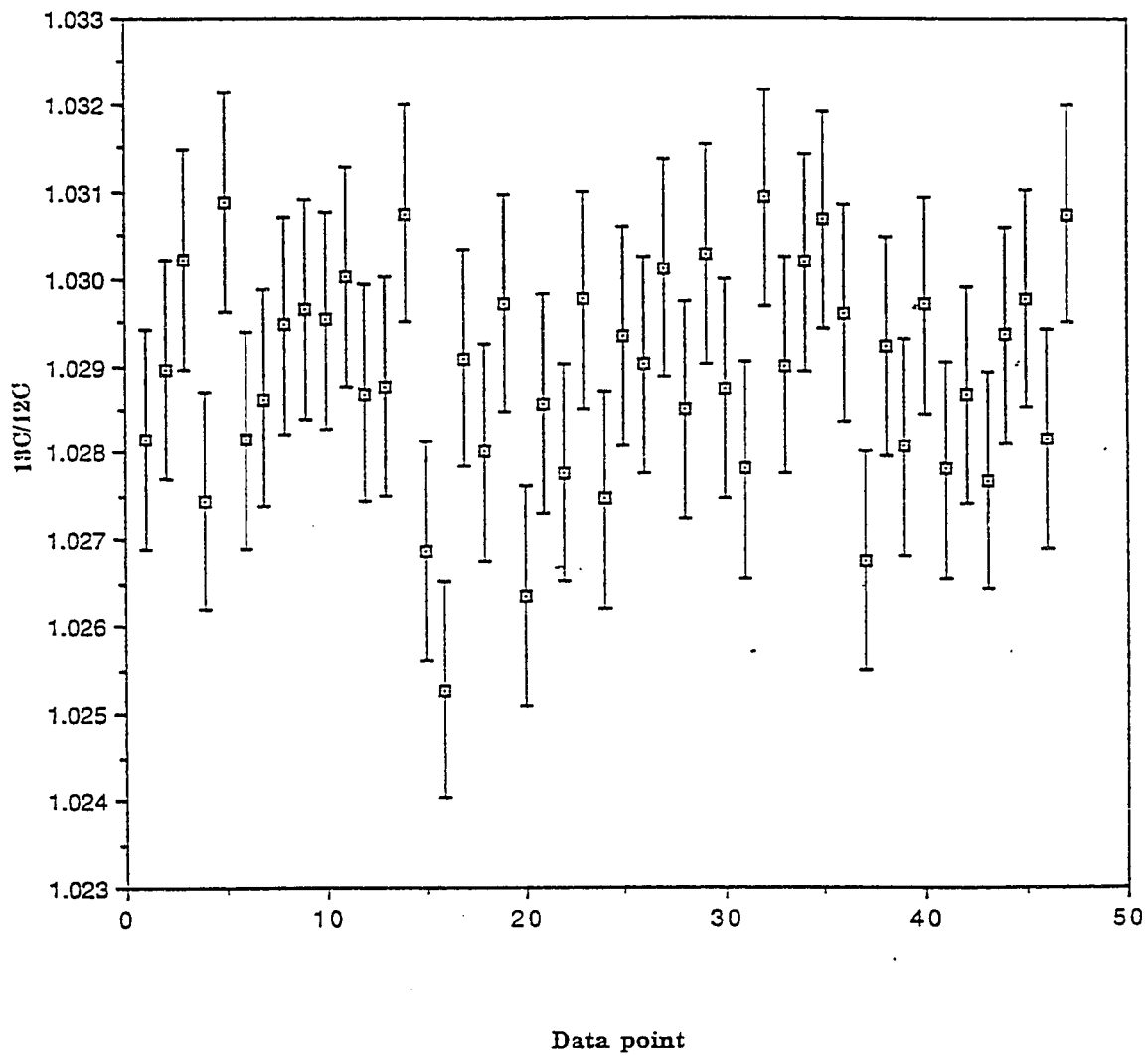


Figure 20: A scatter plot of all data sequences together. These data taken as a constant have a standard deviation of $\pm 0.125\%$.

Chapter 8

References

1. Freund, F., "Solute Carbon and Carbon Segregation in Magnesium Oxide Single Crystals -- a Secondary Ion Mass Spectroscopy Study," *Physics and Chemistry of Minerals*, vol. 13, p. 262-276, 1985 .
2. Kathrein, H., H. Gonska , and F. Freund, "Subsurface Segregation and Diffusion of Carbon in Magnesium Oxide," *Applied Physics*, vol. 30A, p. 33-41, 1983.
3. Sauke, T. B., J. F. Becker, T. D. Gutierrez, and C. G. Bratton, "Improved Stable Isotope Laser Spectrometer and its Application to Soil Analysis," *Proceedings of the Conference on Novel Lasers and Applications*, edited by J. F. Becker, A. C. Tam, J. B. Gruber, and L. Lam, Bellingham: SPIE, 1994.
4. Freund, F., E. Whang, F. Batllo, L. Desgranges, C. Desgranges, and M. M. Freund, "Positive Hole-Type Charge Carriers in Oxide Materials," *Grain Boundaries and Interfacial Phenomena in Electronic Ceramics*, edited by P. Levinson, American Ceramics Society, 1994.

5. Freund, F., M. M. Freund, and F. Batllo, "Critical Review of Electrical Conductivity Measurements and Charge Distribution Analysis of Magnesium Oxide," *Journal of Geophysical Research*, vol. 98, p. B12, 1993.
6. Trice, J. P., "Experimental Determination of Carbon Impurities in Magnesium Oxide Using Ultra-High Resolution Infrared Tunable Diode Laser Spectroscopy," Master's Thesis, Physics Department, San Jose State University, 1991.
7. Nowotny, J., "Surface and Grain Boundary Segregation in Metal Oxides," *Surfaces and Interfaces of Ceramic Materials*, Amsterdam: Kluwer Academic Publishing, 1989.
8. Crank, J., *The Mathematics of Diffusion*, Oxford: Clarendon Press, 1975.
9. Jost, W., *Diffusion in Solids, Liquids, Gases*, New York: Academic Press, 1960.
10. Allnatt A. B., and A. B. Lidiard, *Atomic Transport in Solids*, Cambridge: Cambridge University Press, 1993.
11. Press, W. H., R. P. Flannery, and S. A. Teukolsky, W. T. Vetterling, *Numerical Recipes, The Art of Scientific Computing*, New York: Cambridge University Press, 1986.
12. Garcia, A. L., *Numerical Methods for Physics*, Englewood Cliffs: Prentice-Hall, 1994.

13. Becker, J. F., T.B. Sauke, and M. Loewenstein, "Stable Isotope Analysis Using Diode Laser Spectroscopy," *Applied Optics*, vol. 31, p. 1921-1927, 1992.
14. Sauke, T. B., J. F. Becker, M. Loewenstein, T. D. Gutierrez, and C. G. Bratton, "An Overview of Isotopic Analysis Using Tunable Diode Laser Spectrometry," *Spectroscopy*, vol. 9, no. 5, p. 34-40, June 1994.
15. Dinh, V. V., "Improvement of Tunable Diode Laser Spectrometer IRF," Master's Thesis, Physics Department, San Jose State University, 1992.
16. Sauke, T. B., J.R. Podolske, and T.D. Gutierrez, working title: "Measurement of Lorentzian Laser Linewidths," manuscript in progress, 1994.
17. Schalow, A. L., and C.H. Townes, "Infrared and Optical Masers," *Physical Review*, vol. 112, p. 1940-1949, 1958.
18. Freund, F., personal communication regarding results of reference 2, 1994.
19. Freund, F., personal communication regarding the relevance of MgO sample age, 1994.
20. Freund, F., personal communication regarding expected results, 1994.
21. Sauke, T. B., personal communication regarding improvement of the diffusion model, 1994.